# COMPUTATION OF ENTROPY GENERATION IN DISSIPATIVE TRANSIENT NATURAL CONVECTIVE VISCOELASTIC FLOW

**Mahesh Kumar[1], G. Janardhana Reddy[1,\*], G. Ravi Kiran[2], M.A. Mohammed Aslam[3] and O. Anwar Beg[4]**

[1]*Department of Mathematics, Central University of Karnataka, Kalaburagi, India.*

[2]*Department of Mathematics, SR Engineering College, Warangal, India.*

[3]*Department of Geology, Central University of Karnataka, Kalaburagi, India.*

[4]*Fluid Mechanics, Aeronautical and Mechanical Engineering Department, School of Computing,*

*Science and Engineering, University of Salford, Manchester M54WT, UK*

[\*]*Corresponding author- Email:* gjr@cuk.ac.in

## Abstract

Entropy generation is an important aspect of modern thermal polymer processing optimization. Many polymers exhibit strongly non-Newtonian effects and dissipation effects in thermal processing. Motivated by these aspects in this article a numerical analysis of the entropy generation with viscous dissipation effect in an unsteady flow of viscoelastic fluid from a vertical cylinder is presented. The Reiner-Rivlin physical model of grade two (second grade fluid) is employed which can envisage normal stress variations in polymeric flow-fields. Viscosity variation is included. The obtained governing equations are resolved using implicit finite difference method of Crank-Nicolson type with well imposed initial and boundary conditions. Key control parameters are the second-grade viscoelastic fluid parameter ($\beta$), viscosity variation parameter ($\gamma$) and viscous dissipation parameter ($\varepsilon$). Also, group parameter ($Br\Omega^{-1}$), Grashof number ($Gr$) and Prandtl number ($Pr$) are examined. Numerical solutions are presented for steady-state flow variables, temperature, time histories of friction, wall heat transfer rate, entropy and Bejan curves for distinct values of control parameters. The results specify that entropy generation decreases with augmenting values of $\beta$, $\gamma$ and $Gr$. The converse trend is noticed with increasing $Pr$ and $Br\Omega^{-1}$. Furthermore, the computations reveal that entropy and Bejan lines only occur close to the hot cylinder wall.

**Keywords:** vertical cylinder; second-grade fluid; buoyancy-driven flow; entropy generation; finite difference method; viscous dissipation.

## 1. Introduction

Exterior boundary layer flows with heat transfer are fundamental to numerous processes arising in the process chemical industry and manufacturing systems. In many systems, the surface is curved and typical examples include conical bodies, spheres, ellipses and cylinders. The last of these configurations i.e. the cylinder features in numerous convective flow operations including heat exchangers, clarifying suspensions using filtration screens, to handle hot wire, steam pipe, polymer fiber spinning, a coating of wires, mixing processes, nanotechnology etc. Free convection i.e. wherein buoyancy forces are prominent is also of great interest in such systems [1]. The effects induced by the body curvature are more pronounced at small and moderate Grashof numbers. In the layer neighbouring to the surface, the dominant mechanism of heat transfer is thermal conduction. Furthermore, heat transfer rates at the surface of curved bodies strongly influence the cooling rate which can impact significantly on the constitution of manufactured materials (e.g. plastics, powder). Although many excellent studies of external free (natural) convection to Newtonian fluids have been communicated, there is an extensive spectrum of industrial working fluids which differ from the Newtonian (Navier-Stokes) model. Examples of non-Newtonian fluids in thermal processing include plastics, gels, paints, biotechnological products, powder type creams, medicines, adhesives etc. In the thermally-assisted polymeric coating of pipes and other cylindrical configurations, the boundary layer flow of non-Newtonian from a vertical cylinder becomes an essential problem for engineering analysis. This case (among others) has been reviewed lucidly and quite recently by Chhabra [2] in which a diverse range of non-Newtonian models are considered including power-law fluids, yield stress fluids, thixotropic fluids etc. Non-Newtonian boundary layer flows from cylindrical bodies with and without heat transfer have also been addressed in some detail by a number of other researchers. The inherently nonlinear nature of the transport equations in these studies generally necessitates a numerical solution methodology. Mitsoulis and Galazoulas [3] used a modified Herschel–Bulkley model and a finite element method to compute viscoplastic flows from a cylinder. Chhabra *et al.* [4] used a second-order precise finite difference method to compute iso-vorticity patterns and drag coefficients for both dilatant and pseudoplastic power-law flow from a circular cylinder. Prasad *et al.* [5] premeditated numerically the free convection boundary layer flow from a cylinder to a Jeffreys viscoelastic fluid with Keller's box scheme. Rao *et al.* [6] analysed computationally the laminar thermal magneto-convection with strong buoyancy forces from a cylinder to a Williamson shear-thinning viscoelastic fluid. Bég *et al.* [7] presented numerical solutions for surface characteristics (skin friction, Nusselt

number) of an electro-conductive viscoplastic nanofluid in natural convection from a cylinder under a magnetic field.

In many polymeric heat transfer processes, whether laminar or turbulent, viscous heating effects can become significant. Viscous dissipation produces an appreciable elevation in the fluid temperatures as a result of the conversion of kinetic energy to thermal energy. Polymeric flows are highly viscous and therefore considerable heat can be produced even at relatively low speeds encountered in, for example, the extrusion of polymeric melts and solutions, the production of emulsions and pastes, and the process heating or cooling of viscous gels. Heat transfer results may, therefore, be significantly modified due to viscous dissipation. Viscous dissipation in non-Newtonian flows has been extensively investigated in the literature. Kairi *et al.* [8] considered variable-viscosity rheological flows in porous media. They presumed that the fluid viscosity is followed by the Reynolds viscosity model. Ragueb and Mansouri [9] analysed computationally the viscous heating in laminar heat transfer of power-law fluids inside elliptical cross-section ducts with uniform wall temperature through dADI technique. Their study addresses Nusselt number modification with various values of Brinkman number (viscous dissipation parameter) and the aspect ratio of the duct. Manglik and Prusa [10] presented asymptotic boundary-layer-scaled finite difference solutions for viscous dissipation impacts on thermal convection in power-law fluid flows in constant wall temperature tubes. They concluded that Brinkman number effects are vital predominantly in a transition region. Further studies of dissipative thermal convection include Shamshuddin *et al.* [11] for micropolar fluids on inclined surfaces, Ali *et al.* [12] for Giesekus viscoelastic fluids in wire coating, Zaib et al. [13] and Barletta [14] for power-law fluids. These studies have generally shown that omission of viscous heating effects tends to under-predict temperatures and over-predict velocity distributions and therefore furnishes unrealistic information on thermal/fluid characteristics which may be detrimental to polymer processing design.

In the above studies, many different rheological formulations have been implemented. However, another group of nonlinear models is available, namely differential fluids. Introduced initially by Coleman and Noll [15], this subclass of viscoelastic fluids includes the Rivlin-Ericksen fluid of grade two or second-grade fluid and also the third grade and fourth grade fluid models. Among those second-grade fluid model is capable of describing the effects of normal stress in polymeric flow-fields (McTigue *et al.* [16]). This model has received considerable attention among applied mathematicians and engineers. It has been deployed to simulate slurry flows, molten plastics, dilute polymer solutions, polymer melts like

manufacturing oils and high-viscosity silicone oils. Numerous well-posed boundary value problems are analysed with the second-grade fluid model. The influence of viscous dissipation on hydromagnetic second-grade fluid flow with convective heat and mass transfer over a sheet was considered by Das [17]. Nadeem *et al.* [18] analysed the second-grade fluid flow problem in a cylinder by considering viscous dissipation effect and obtained the analytical solution using boundary layer approximation. Hayat *et al.* [19] scrutinized the second-grade fluid flow with MHD from a permeable stretching cylinder. Their investigation has been conceded for heat and mass transfer with viscous dissipation and Joule effects. Nayak and Panda [20] examined the hydromagnetic second-grade fluid flow with the effect of viscous dissipation and Joule heating over a vertical plate. They showed that flow-field variables are enhanced with higher Eckert number. Bikash Sahoo [21] examined the heat transfer of a second-grade MHD fluid flow from a stretching sheet with the effect of viscous dissipation, slip and Joule heating. Recently, Majeed *et al.* [22] evaluated cross-diffusion i.e. Soret and Dufour impact on 2-D second-grade fluid flow from stretching cylinder by elaborating the impact of radiation effects through an effective Prandtl number.

Thermodynamic optimization of engineering systems has emerged as a significant area of recent investigation, primarily motivated by increasing efficiency and sustainability of 21$^{st}$ century technologies. The designs of flow and heat transfer systems are based on thermodynamics laws. First law of thermodynamics which dictates that energy in a system is not lost, but it is transmitted from one medium to another or it is transferred from one form to another. However, first law doesn't account for irreversibilities (entropy generation). Second law analysis enumerates the collection and useful consumption of available energy and identifies the unrecoverable losses, leading the way to enlightening the thermodynamic performance system. It can be used together with energy analysis and minimizes the available energy loss. Bejan [23] described the entropy generation concept as a new analysis for the thermodynamics which consists of taking into account the first and second law. The entropy heat generation has been used in the study of cryogenics, turbo-machinery, porous media, combustion, electronic cooling, and rotating disk reactors. Remarkable recent works deploying thermodynamic second law include modelling of solar heat exchangers (Giangaspero and Sciubba [24]), lost exergy during heat transfer processes (Badescu [25]), multi-field flows (Kockum and Jernqvist [26]), nuclear swirl electromagnetic propulsion (Rashidi *et al.* [27]), hydromagnetic annular non-Newtonian flows (Jangili *et al.* [28]), analysing reactive polar fluids for channel flow (Adesanya *et al.* [29]) and carbon nanotube-nanofluid dynamic via cilia-

assisted porous medium (Akbar *et al.* [30]). Further articles considering entropy generation of non-Newtonian fluids include Aksoy [31], Galanis and Rashidi [32], Kahraman [33] and Sajjad-ur *et al.* [34]). Further, several simulations have been conducted for entropy generation with viscoelastic fluids. Butt *et al.* [35] discussed the consequence of entropy generation for second-grade from a plate in a porous medium. Yilbas and Pakdemirli [36] analysed the entropy generation for non-Newtonian fluid flow in a circular pipe. Also, the entropy concept for third grade fluid flow in an annular pipe was studied by Yurusoy et al. [37]. Other recent studies can be found in Ref. [38-39].

From aforesaid data, it is apparent that limited number of work has been afforded thus far to entropy generation in time-dependent viscoelastic flows external to curved geometries. Motivated by applications to the polymer processing industry, in the current research work a numerical study is conducted for second-grade elastico-viscous free convection flow from a uniformly heated vertical cylinder. Other important characteristics of polymers are viscous heating and temperature-dependent viscosity. Viscous dissipation has also been shown to be very prominent in thermo-polymeric synthesis as highlighted in Xu *et al.* [40]. Both viscous dissipation and temperature-dependent viscosity are therefore considered in the present study. Thus, in general, recourse must be made to efficient numerical methods. In this work, the Crank-Nicolson implicit finite difference method is utilized to solve the transformed, dimensionless, unsteady second-grade boundary layer equations and computations are corroborated with previously published results available in the literature. Furthermore, the results obtained for second-grade fluids are compared with the Newtonian fluid case.

## 2. Problem description

The time-dependent 2-D laminar free convection flow of a polymeric second-grade viscoelastic fluid from a heated vertical cylinder of radius $r_0$ has been considered and illustrated in **Fig. 1**. The considered coordinate structure is in rectangular form, in which the axial (*x*) and radial (*r*) coordinate axes are selected from the base edge and normal to the cylinder respectively. The adjacent fluid temperature is taken to be stationary i.e. constant (fixed) temperature and similar to that of ambient temperature, $T'_\infty$ . At the outset, i.e. $t' = 0$, the temperature $T'_\infty$ is uniform for the cylinder and the fluid. Later ($t' > 0$), the cylinder temperature is augmented to $T'_w (> T'_\infty)$ and conserved consistently there afterward.

The Cauchy stress tensor **T** for a second-grade viscoelastic fluid (Fosdick and Rajagopal [41], Rajagopal and Gupta [42]) is given by:

$$\mathbf{T} = -P\mathbf{I} + \mu \boldsymbol{B}_1 + \alpha_1 \boldsymbol{B}_2 + \alpha_2 \boldsymbol{B}_1^2 , \tag{1}$$

where $P$, **I**, $\mu$ and $\alpha_i's$ $(i = 1, 2)$ characterise the pressure, identity tensor, material constants and dynamic viscosity, respectively. Also $\boldsymbol{B}_1$, $\boldsymbol{B}_2$ are the Rivlin–Ericksen tensors and are given by $\boldsymbol{B}_1 = (\text{grad } \boldsymbol{V}) + (\text{grad } \boldsymbol{V})^{\mathrm{T}}$, $\boldsymbol{B}_2 = \frac{\mathrm{d}\boldsymbol{B}_1}{\mathrm{dt}} + \boldsymbol{B}_1(\text{grad } \boldsymbol{V}) + (\text{grad } \boldsymbol{V})^{\mathrm{T}}\boldsymbol{B}_1$ , in which $grad$ is the gradient operator, $\frac{\mathrm{d}\boldsymbol{B}_1}{\mathrm{dt}}$ is the material time derivative and $\boldsymbol{V}$ is the velocity vector. The constants $\alpha_1, \alpha_2$ represent normal stress moduli. Eq. (1) is to be consistent with thermodynamics in the sense that all the fluid motions satisfy Clausius-Duhem inequality and the hypothesis that the specific Helmholtz free energy of the fluid is a minimum in equilibrium, then (Dunn and Rajagopal [43]).

$$\mu \geq 0, \quad \alpha_1 \geq 0, \quad \alpha_1 + \alpha_2 = 0. \tag{2}$$

Using the inequality and restrictions in Eqn. (2), the governing time-dependent equations with assumptions made by Boussinesq's are as follows:

$$\frac{\partial (r\,u)}{\partial x} + \frac{\partial (r\,v)}{\partial r} = 0, \tag{3}$$

$$\frac{\partial u}{\partial t'} + u\frac{\partial u}{\partial x} + v\frac{\partial u}{\partial r} = g\beta_T(T' - T'_\infty) + \frac{1}{\rho}\frac{\partial}{\partial r}\frac{1}{r}\left(\bar{\mu}r\frac{\partial u}{\partial r}\right)$$

$$+ \frac{\alpha_1}{\rho}\left(\begin{array}{c}\frac{\partial^3 u}{\partial r^2 \partial t'} + \frac{1}{r}\frac{\partial^2 u}{\partial r \partial t'} + \frac{\partial u}{\partial x}\frac{\partial^2 u}{\partial r^2} + u\frac{\partial^3 u}{\partial x \partial r^2} + v\frac{\partial^3 u}{\partial r^3} - \frac{\partial u}{\partial r}\frac{\partial^2 v}{\partial r^2} + \frac{\partial u}{\partial r}\frac{\partial^2 u}{\partial x \partial r} \\ + \frac{1}{r}\left(v\frac{\partial^2 u}{\partial r^2} + u\frac{\partial^2 u}{\partial x \partial r} - \frac{\partial v}{\partial r}\frac{\partial u}{\partial r} + \frac{\partial u}{\partial x}\frac{\partial u}{\partial r}\right)\end{array}\right), \tag{4}$$

$$\frac{\partial T'}{\partial t'} + u\frac{\partial T'}{\partial x} + v\frac{\partial T'}{\partial r} = \frac{\alpha}{r}\frac{\partial}{\partial r}\left(r\frac{\partial T'}{\partial r}\right) + \frac{\bar{\mu}}{\rho c_p}\left(\frac{\partial u}{\partial r}\right)^2 + \frac{\alpha_1}{\rho c_p}\left(\frac{\partial^2 u}{\partial r \partial t'}\frac{\partial u}{\partial r} + u\frac{\partial u}{\partial r}\frac{\partial^2 u}{\partial x \partial r} + v\frac{\partial u}{\partial r}\frac{\partial^2 u}{\partial r^2}\right). \tag{5}$$

where $u, v$ are the velocity constituents along axial $(x)$ and radial $(r)$ coordinate systems, respectively, $\rho$ is the fluid density $\beta_T$ - volumetric thermal expansion coefficient, $c_p$ is the specific heat at constant pressure, $T'$ - temperature, g - acceleration due to gravity, $T'_\infty$ - free stream temperature.

The related initial and boundary conditions are given by:

$t' \leq 0: \quad T' = T'_\infty, v = 0, u = 0 \qquad\qquad$ for all $x$ and $r$

$t' > 0: \quad T' = T'_w, v = 0, u = 0 \qquad\qquad$ at $r = r_0$

$$T' = T'_\infty \; , \; v = 0, u = 0 \qquad \text{at } x = 0 \qquad\qquad (6)$$

$$T' \to T'_\infty \; , v \to 0, u \to 0, \frac{\partial u}{\partial r} \to 0 \qquad \text{as } r \to \infty \;.$$

Invoking the following non-dimensional quantities:

$$X = Gr^{-1}\frac{x}{r_0} \;,\; T = \frac{T'-T'_\infty}{T'_w-T'_\infty}, \quad R = \frac{r}{r_0}\;, U = Gr^{-1}\frac{ur_0}{v}, \; V = \frac{vr_0}{v}, \quad t = \frac{vt'}{r_0^2}, \; Gr = \frac{g\beta_T r_0^3 (T'_w - T'_\infty)}{v^2},$$

$$Pr = \frac{v}{\alpha}\;,\; \beta = \frac{\alpha_1}{\rho r_0^2}, \; v = \frac{\mu_\infty}{\rho}\;, Br = \frac{\mu_\infty v^2}{k(T'_w - T'_\infty)r_0^2}\;, \; \Omega = \frac{(T'_w - T'_\infty)}{T'_\infty} \;, \varepsilon = \frac{v^2}{c_p(T'_w - T'_\infty)r_0^2}\;. \qquad (7)$$

where $U, V$ are the dimensionless velocity components along $X$ and $R$ direction, respectively, $\alpha$ - thermal diffusivity, $\varepsilon$ - viscous dissipation parameter, k - thermal conductivity, $\mu$ - viscosity of the fluid, $v$ - kinematic viscosity, Br - Brinkman number, Gr - Grashof number, $\Omega$ - dimensionless temperature difference, Pr - Prandtl number, $\beta$ – viscoelastic parameter, $Br\Omega^{-1}$ - group parameter.

There are several types of viscosity variations exist in the nature, among those we have considered one of the form proposed by Cengel [44] and Touloukian *et al.* [45]):

$$\overline{\mu}(T') \cong \mu_\infty(1 + \lambda(T' - T'_\infty)), \qquad\qquad (8)$$

where $\overline{\mu}$ is the fluid viscosity subject to temperature $T'$ and $\mu_\infty$ denotes fluid viscosity at the temperature $T'_\infty$. Let $\gamma$ represent the non-dimensional viscosity variation parameter defined by $\gamma = \lambda(T'_w - T'_\infty)$. Here $\lambda$ dimensional viscosity variation parameter. It follows that the viscosity of the second-grade fluid as a function of dimensionless temperature can be written as:

$$\overline{\mu}(T) = \mu_\infty(1 + \gamma T) \;. \qquad\qquad (9)$$

Invoking the above cited non-dimensional numbers in Eqns. (3) - (5) and also in the conditions defined in Eqn. (6), the transport equations contract to the following form:

$$\frac{\partial U}{\partial X} + \frac{\partial V}{\partial R} + \frac{V}{R} = 0 \;, \qquad\qquad (10)$$

$$\frac{\partial U}{\partial t} + U\frac{\partial U}{\partial X} + V\frac{\partial U}{\partial R} = \text{T} + (1 + \gamma T)\left(\frac{\partial^2 U}{\partial R^2} + \frac{1}{R}\frac{\partial U}{\partial R}\right) + \gamma\frac{\partial T}{\partial R}\frac{\partial U}{\partial R}$$

$$+\beta\left(\begin{array}{c}\frac{\partial^3 U}{\partial R^2 \partial t} + \frac{1}{R}\frac{\partial^2 U}{\partial R \partial t} + \frac{\partial U}{\partial X}\frac{\partial^2 U}{\partial R^2} + U\frac{\partial^3 U}{\partial X \partial R^2} + V\frac{\partial^3 U}{\partial R^3} - \frac{\partial U}{\partial R}\frac{\partial^2 V}{\partial R^2} + \frac{\partial U}{\partial R}\frac{\partial^2 U}{\partial X \partial R} \\ + \frac{1}{R}\left(V\frac{\partial^2 U}{\partial R^2} + U\frac{\partial^2 U}{\partial X \partial R} - \frac{\partial V}{\partial R}\frac{\partial U}{\partial R} + \frac{\partial U}{\partial X}\frac{\partial U}{\partial R}\right)\end{array}\right), \quad (11)$$

$$\frac{\partial T}{\partial t} + U\frac{\partial T}{\partial X} + V\frac{\partial T}{\partial R} = \frac{1}{Pr}\left(\frac{\partial^2 T}{\partial R^2} + \frac{1}{R}\frac{\partial T}{\partial R}\right) + (Gr)^2\varepsilon(1+\gamma T)\left(\frac{\partial U}{\partial R}\right)^2$$

$$+(Gr)^2\varepsilon\beta\left(\frac{\partial^2 U}{\partial R\partial t}\frac{\partial U}{\partial R} + U\frac{\partial U}{\partial R}\frac{\partial^2 U}{\partial X\partial R} + V\frac{\partial U}{\partial R}\frac{\partial^2 U}{\partial R^2}\right), \tag{12}$$

$$
\begin{array}{llll}
t \leq 0: & T = 0\,, V = 0, U = 0 & \text{for all } X \text{ and } R \\
t > 0: & T = 1\,, V = 0\,, U = 0 & \text{at } R = 1 \\
 & T = 0\,, V = 0\,, U = 0 & \text{at } X = 0 \\
 & T \to 0\,, V \to 0, U \to 0, \frac{\partial U}{\partial R} \to 0 & \text{as } R \to \infty\,.
\end{array} \tag{13}
$$

## 3. Finite difference numerical solution

To solve the time-dependent mathematical flow model defined by Eqns. (10) - (12) along with initial and boundary conditions (13), the popular finite difference Crank-Nicolson method is applied which is described in [46]. It has been applied in analysis of viscoelastic flows (Walters-B liquids) by Mohiddin *et al.* [47] for transient double-diffusive convection from a cone and Prasad *et al.* [48] for time-dependent free convective flow from plate. More recently this method has been used in computing magnetic nanofluid flows from translating cylindrical bodies with periodic temperature variation (Rajesh *et al.* [49]) and radiative-convective nanofluid flow from a cylinder (Rajesh *et al.* [50]). The zone of integration formed as a rectangular with sides $X_{max} = 1$, $X_{min} = 0$, $R_{max} = 20$ and $R_{min} = 1$, where $R_{max}$ relates to $R = \infty$ which lies distant from the energy and momentum boundary layers. Also, the accuracy of the present computational results are compared with the erstwhile studies (Newtonian fluid) of Lee *et al.* [51] for $Pr = 0.7$, $\beta = 0, \gamma = 0$ and $\varepsilon = 0$, and it is found to be in good agreement which is shown in Figure 2. Further, to validate the Crank-Nicolson method for the present study on non-Newtonian second-grade fluid model, the authors considered different physical model on second-grade fluid [52] and implemented the same Crank-Nicolson method to get the numerical results for their study. These results are well agreed with Mustafa *et al.* [52] and shown in Figure 3. Therefore, it is concluded that confidence in the present Crank-Nicolson code is justifiably high and that the present numerical results demonstrate sufficiently high accuracy.

## 4. Grid independence study for numerical code

To achieve an economical and stable grid structure for computation, a grid independency assessment is done over the values of the $\overline{Nu}$ for different grid sizes with fixed time step size $\Delta t = 0.01$ and for distinct time step sizes with fixed grid 100 x 500, which are documented in **Table 1** and **Table 2,** respectively.

## 5. Results and discussion

The description of governing flow-field results are plotted with fixed value of Grashof number $(Gr = 1)$, various physical parameter values namely second-grade fluid parameter ($\beta$), viscosity variation parameter ($\gamma$), viscous dissipation parameter ($\varepsilon$), group parameter ($Br\Omega^{-1}$) and Prandtl number ($Pr$) in succeeding Figures.

### 5.1 Velocity and temperature variables

**Figure 4(a)** describe the unsteady velocity distribution at the spatial coordinate (1, 3.2) which plotted $U$ against $t$ for individual $\beta$, $\gamma$ and $\varepsilon$ values. Evidently, the fluid velocity is augmented with $t$, attains its peak, then slightly declines and finally attains the time-independent (steady) state value. For instance, when $\beta = 1.0$, $\gamma = 0.2$ and $\varepsilon = 1.0$ the velocity monotonically augments with time and accomplishes the temporal peak $(U = 0.439)$ at $t = 5.35$ then marginally reduces and finally turn out to be asymptotically steady $(U = 0.39)$. At the outset when $t \ll 1$, describes the conduction dominates over the convection. Also, overshoots of the velocities are noticed in this figure. This is due to particular values of dimensionless viscosity $(1 + \gamma T)$ and dimensionless thermal diffusivity $1/Pr$ is possibly the reason for the overshoot of the velocity. The transient velocity, $U,$ profile increases with increasing $\beta$ values, the flow is accelerated since higher elastic impacts are generated as per the delineation of this viscoelastic parameter $= \frac{\alpha_1}{\rho r_0^2}$). This strengthens the flow and assists momentum development. Also, this transient $U,$ profile at the outset decreases with increasing $\gamma$. Fluid viscosity is increased with higher $\gamma$ and this enhances viscous forces in the momentum boundary layer which deaccelerates the flow (viscous i.e. momentum diffusion is strongly affected at a given Prandtl number). Similarly, there is a boost in velocity with increasing dissipation parameter ($\varepsilon$). It is also noteworthy that the required time to accomplish the temporal peak rises as $\gamma$ increases whereas for increasing $\beta$ and $\varepsilon$ values the trend is reversed. Very different responses in time are therefore computed with variation in these three viscosity-related parameters.

**Figure 4(b)** portrays the distribution of unsteady temperature profile ($T$) plotted at the spatial coordinate (1, 1.15) for the values of β, γ and ε. Temperature clearly is emphasized initially with time, achieves an extreme value and thereafter is weakly reduced; finally, attain the steady-state. Initially, temperature curves coincide with each other for all values of control parameters and deviated after some intervals. Temperature is clearly enhanced with superior values of γ and β. The effect of viscoelastic parameter β is less as compared to viscosity variation parameter γ. The reason is that as γ upsurges the fluid viscosity increases which allow higher temperature profile. The increase in the fluid temperature is being caused by stronger elastic forces in the medium and also a change in viscosity which boosts motion of the fluid particle. Increasing viscous dissipation parameter (ε), as anticipated, strongly elevates the temperature. This is due to a boost in the thermal energy generated by kinetic energy dissipation as a result of flow against resistance forces, and is an observation confirmed in many other studies, notably Gebhart [53]. The inclusion of viscous dissipation effects is therefore important since it avoids under-prediction of temperatures associated with non-dissipative models. This has implications for wall cooling rates also which are critical in polymer (and other) materials processing operations.

**Figure 5(a)** reveals the response in dimensionless steady-state axial velocity profiles for various governing parameters (β, γ and ε) against radial coordinate, $R$. The velocity, $U$ commences with zero value, accomplishes its maximum and then decays to zero with increasing $R$ coordinate sustaining the far-field (free stream) boundary conditions. Besides, in the vicinity of the cylindrical wall, the magnitude of $U$ profile is augmented with greater $R$ values, achieving a peak near to the cylindrical surface into the boundary layer. The peak is displaced away from the cylinder surface with increasing γ. Also, the required time to complete the steady-state decreases for increasing γ or β and the opposite behaviour is computed with increasing dissipation parameter, ε. Further, it is also noted that, as β and γ increase, the peak velocity magnitude is diminished. Additionally, for the higher viscosity case, the motion of the fluid occurs slowly near the hot wall while the fluid with lesser viscosity, the fluid motion is speed up nearby wall. Hence it is obvious that in the environs of the cylinder the velocity magnitude is high for γ compared to β and ε i.e. γ has a more reflective accelerating impact on axial velocity.

**Figure 5(b)** Illustrates the steady-state temperature ($T$) distributions versus $R$ for distinct values of β, γ and ε. These outlines initiate with the boundary value of $T = 1$ and then reduce to zero

as $R$ increases. It is noted that, with greater viscosity parameter ($\gamma$), there is a significant eventual elevation in temperature i.e. the regime is energized and the thermal boundary layer thickness is also increased. A similar pattern is induced with augmenting values of viscous dissipation parameter ($\varepsilon$) which again implies thicker the thermal boundary layer development. It is also pertinent to highlight that the time-independent state $T$ curves demonstrate a very little deviation from each other indicating that viscoelastic parameter ($\beta$) exerts a trivial influence on thermal field. The viscoelastic effect is primarily confined to velocity field. There are no viscoelastic terms in the momentum eqn. (11) for the second-grade model. However, in higher models of the differential type (e.g. third grade model), viscoelastic terms do feature in the momentum equation, and as such impart a significant effect on temperatures, as elaborated by Bég *et al.* [54].

**5.2 Friction and heat transport coefficients**

From the velocity and temperature flow-fields, the mathematical expressions for skin friction and Nusselt number are determined easily. They are used to measure of the wall shear stress heat transfer rate at the boundary. The skin-friction $\overline{C_f}$ and Nusselt number $\overline{Nu}$ can be written as:

$$\overline{C_f} = (1 + \gamma) \int_0^1 \left(\frac{\partial U}{\partial R}\right)_{R=1} dX \quad \text{and} \quad \overline{Nu} = -\int_0^1 \left(\frac{\partial T}{\partial R}\right)_{R=1} dX. \tag{14}$$

**Figures 6(a) - 6(b)** elucidate the average momentum and wall heat transfer which are plotted against time ($t$) with a variation in $\beta$, $\gamma$ and $\varepsilon$ parameters. Figure 6(a) displays that $\overline{C_f}$ increases considerably with $t$ and after a certain lapse of a period it attains the steady-state region. Also, there is a substantial reduction in $\overline{C_f}$ with $\gamma$ as a result of slowing down in the flow with effects higher viscosity. This is also consistent with the time-dependent $U$ graph as described earlier in Fig. 4(a). Also, boosting values of $\beta$ and $\varepsilon$ both evident in a marked lessening in $\overline{C_f}$ *i.e.* a strong deceleration at the wall is induced with stronger viscoelastic and dissipative effects.

**Figure 6(b)** illustrates that initially, the magnitude of wall heat transfer gradient i.e. $\overline{Nu}$ decreases drastically, a tendency which is pursued by a trivial escalation in magnitudes and eventual accomplishment of the time-independent state. Also, it is noted that initially, the $\overline{Nu}$ curves coincide with each other and only deviated from each other after some elapse in time.

It is also obvious that $\overline{Nu}$ decreases with accumulative values of β, γ and ε, which is physically consistent with an increase in temperatures in the boundary layer (computed earlier).

### 5.3 Computation of entropy heat generation and Bejan number

The entropy generation expression for an incompressible second-grade fluid is given by:

$$S_{gen} = \frac{k}{T_\infty'^2}\left(\frac{\partial T'}{\partial r}\right)^2 + \left\{\frac{\bar{\mu}}{T_\infty'}\left(\frac{\partial u}{\partial r}\right)^2 + \frac{\alpha_1}{T_\infty'}\left[\frac{\partial^2 u}{\partial r \partial t'}\frac{\partial u}{\partial r} + v\frac{\partial u}{\partial r}\frac{\partial^2 u}{\partial r^2} + u\frac{\partial u}{\partial r}\frac{\partial^2 u}{\partial x \partial r}\right]\right\} \tag{15}$$

Eqn. (15) can be re-written as:

$$S_{gen} = S_1 + S_2 \tag{16}$$

Here:

$$S_1 = \frac{k}{T_\infty'^2}\left(\frac{\partial T'}{\partial r}\right)^2, \quad S_2 = \frac{\bar{\mu}}{T_\infty'}\left(\frac{\partial u}{\partial r}\right)^2 + \frac{\alpha_1}{T_\infty'}\left[\frac{\partial^2 u}{\partial r \partial t'}\frac{\partial u}{\partial r} + v\frac{\partial u}{\partial r}\frac{\partial^2 u}{\partial r^2} + u\frac{\partial u}{\partial r}\frac{\partial^2 u}{\partial x \partial r}\right] \tag{17}$$

Here $S_1$ and $S_2$ signifies the entropy generation due to by heat flow, and viscous dissipation for incompressible second-grade fluid respectively.

The dimensionless entropy heat generation parameter *Ns* is defined as (Bejan [55]):

$$Ns = \frac{volumetric\ entropy\ generation\ rate}{characteristic\ entropy\ generation\ rate}$$

Thus the entropy generation number for the considered problem can be written as

$$Ns = \left(\frac{\partial T}{\partial R}\right)^2 + \frac{Br(Gr)^2}{\Omega}\left\{(1 + \gamma T)\left(\frac{\partial U}{\partial R}\right)^2 + \beta\left(\frac{\partial^2 U}{\partial R \partial t}\frac{\partial U}{\partial R} + V\frac{\partial U}{\partial R}\frac{\partial^2 U}{\partial R^2} + U\frac{\partial U}{\partial R}\frac{\partial^2 U}{\partial X \partial R}\right)\right\} \tag{18}$$

where characteristic entropy heat generation is $\frac{k(T_w' - T_\infty')^2}{T_\infty'^2 r_0^2}$. The equation (18) can be rephrased in the subsequent form as:

$$Ns = N_1 + N_2 \tag{19}$$

Here

$$N_1 = \left(\frac{\partial T}{\partial R}\right)^2 \text{ and } N_2 = \frac{Br(Gr)^2}{\Omega}\left\{(1 + \gamma T)\left(\frac{\partial U}{\partial R}\right)^2 + \beta\left(\frac{\partial^2 U}{\partial R \partial t}\frac{\partial U}{\partial R} + V\frac{\partial U}{\partial R}\frac{\partial^2 U}{\partial R^2} + U\frac{\partial U}{\partial R}\frac{\partial^2 U}{\partial X \partial R}\right)\right\} \tag{20}$$

$N_1$ and $N_2$ symbolizes the heat transfer irreversibility and fluid friction (viscous dissipation), respectively.

To estimate distribution of the irreversibility [56], the parameter $Be$ (Bejan number) is given by:

$$Be = \frac{N_1}{N_1 + N_2} \tag{21}$$

From Eqn. (21), $0 \leq Be \leq 1$. Subsequently, $Be = 0$ implies that the parameter $N_2$ leads the parameter $N_1$, whereas $Be = 1$ implies that the parameter $N_1$ dominates the parameter $N_2$. It follows that at $Be = 0.5$, the contribution of fluid friction is equal to heat transfer irreversibility i.e. $N_2 = N_1$.

**Figure 7** presents the effect of distinct flow-field control parameters on transient $Ns$ which is drawn against $t$ at the spatial coordinate (1, 1.72). The variation of $\beta$, $\gamma$ and $\varepsilon$ over transient $Ns$ is depicted in Fig. 7(a). From this plot, it is noticed at first, the $Ns$ curves overlap with each other and split afterward for all physical parameters values. This states that in the initial period (i.e., $t < 1.35$) thermal conduction is further dominant than the thermal convection heat transfer. Also the eminent remark from Fig. 7(a) is that $Ns$ decreases with augmenting $\gamma$ and $\beta$. However, $Ns$ is enhanced with greater values of dissipation parameter, $\varepsilon$. This is due to as viscous heating upsurges with augmenting $\varepsilon$, and as a result the fluid particles disorderness increases and hence which leads to higher $Ns$. Fig. 7(a) further indicates that the time to accomplish temporal peak increases for all values of parameters, $Br\Omega^{-1}, Gr$ and $Pr$. The influence of these parameters is significant. Brinkman number expresses the contribution of viscous heat generation by shear to the direct heat conduction from the cylinder surface. Grashof number expresses the contribution of thermal buoyancy force to viscous force. Prandtl number summarizes the ratio of momentum diffusion rate to thermal (energy) diffusion rate. All these parameters enhance the $Ns$ magnitudes as shown in Fig. 7(b). Here the $Ns$ profile trend is almost similar as explained in Fig. 7(a). Hence, from Fig. 7(b) is remarked that amplifying the values of physical parameter shows more entropy production, particularly with boosting group parameter, $Br\Omega^{-1}$.

**Figs. 8(a) - 8(b),** depict the time-independent $Ns$ profiles for distinct control parameters along the $R$ axis at $X = 1.0$. As the $R$ position rises, the $Ns$ magnitudes markedly upsurge, achieve a peak value, then decrease monotonically to zero. Figure 8(a) signifies the variations of $\beta$, $\gamma$ and $\varepsilon$ on the time-independent $Ns$ profiles. The $Ns$ curve peak values are sharpened in the vicinity of the hot cylindrical wall for cumulative values of $\gamma$ and $\beta$. However, the $Ns$ curves are smoother at the maximum value of the dissipation parameter, $\varepsilon$. Further, the viscous dissipation parameter plays a prominent role in the entropy generation effects [Refer Eq. (18)]. Due to this

effect, in Fig. 8(a), the local maximum is observed for the entropy generation. From this graph, it is apparent that for increasing values of γ and β, the steady-state $Ns$ curves decrease nearby the cylindrical surface (i.e., in the interval $R \in [1, 2.15]$), then increase when $R > 2.15$. For escalating values of ε, the curves inter-twine with each other. It is seen that $Ns$ is increased by increasing the values of ε. Additionally, the distribution of $Ns$ is essential in the region nearby the hot cylinder. The cylinder wall has a strong impact on entropy generation due to sudden changes in the temperature difference. Also, the term $(1 + \gamma T)$ is appeared in the equation (18), in which γ is a temperature dependent viscosity. Due to this temperature difference effect, entropy generation shrinkages sharply with increasing radial coordinate $R$. Similar trend can be observed in the available literature for $Ns$ [57-59]. Figure 8(b) depicts that, in the environs of a cylinder surface, the entropy escalates rapidly, then decreases drastically, finally vanishing with large radial coordinate. Further, it is remarked that by boosting values of the control parameter (i.e $Br\Omega^{-1}$, $Gr$ and $Pr$ ), all the $Ns$ curves increase. For larger values of these control parameters, the entropy production due to the fluid friction increases.

The analysis of entropy contours in a given two-dimensional domain using dimensionless $Ns$ is called as entropy visualization (entropy contours). **Figures 9(a) and 9(b)** illustrate the entropy lines with respect to various β and γ values. The deviation of entropy lines very close the hot surface of the cylinder for the variation (viscosity parameter) γ compared to (viscoelastic parameter) β. From both Fig. 9(a) and 9(b) it is seen that, at any spatial coordinate $(X, R)$, the entropy contour value decreases for increasing values of γ and β. Also, entropy contours display lower values for β and higher values for γ. This is true since the entropy production is higher for γ compared to β as demonstrated in Fig. 9(a). Further, entropy contours are not smooth near the cylinder wall. The reason is as explained in the earlier Fig. 8(a); the $Ns$ is not smooth near the hot wall due to the sudden change in the temperature difference. Hence, the entropy contours are also not smooth near the cylinder wall. The essential remark from these figures is that the entropy production occurs in the neighbourhood of the hot cylinder wall only.

**Fig. 10a-b** illustrates the evolution of $Be$ with against time ($t$), for various non-dimensional parameters. These results show that at first $Be$ start with negative value, rises with time, and reaches the peak value, then lastly turn out to be independent of time after a slight oscillation. At the beginning of the flow, the heat transfer irreversibility controls the entropy and when $t > 1.3$ entropy is dominated by fluid friction. From Fig. 10(a) generally, it is seen that as γ or ε

are increased, the Bejan number is enhanced markedly. Also, it is remarked that cumulative β causes a reduction in values in *Be*. From Fig. 10(b) it is noted that as $Br\Omega^{-1}$ or *Gr* rises, the Bejan number upsurges i.e. viscous heating and thermal buoyancy both augment the Bejan number. The opposite trend is induced with increasing *Pr* (i.e. decreasing thermal conductivity of the fluid). Again the taken to attain a time-independent state and temporal peak is almost indistinguishable with increasing values of the combined parameter, $Br\Omega^{-1}$.

**Figs. 11a-b** visualize the steady-state *Be* variation with *R* coordinate at *X* = 1.0 for several values of governing parameter (β, γ, ε, $Br\Omega^{-1}$, *Gr* and *Pr*). In these entire plots, the steady-state features of Bejan number are invariably similar to the steady-state entropy generation (*Ns*) depicted earlier in Figs. 7(a) - 7(b). Particularly, it is noticed that heat transfer irreversibility ensues in the radial direction, i.e., $R \in [2.5, 3.5]$ which reasons negative values in *Be*. Generally, it is seen from Fig. 11(a), that the time-independent state *Be* magnitudes decrease as γ increases and the converse trend is attained with escalating values of β or $\varepsilon$. Also from Fig. 11(b), it is apparent that *Be* is enhanced with superior values of $Br\Omega^{-1}$ and *Gr*. The converse response is computed for increasing Prandtl number, *Pr*. The essential observation is made from these figures is that the time-independent state *Ns* production outstrips the *Be* nearby cylinder surface. This endorses that smaller *Be* yields an increase in $N_2$, i.e., $N_1 \leq, N_2$, and thus irreversibility due to heat transfer is dominated by fluid friction which gives more entropy production in the neighbourhood of the hot cylinder surface (wall).

**Figures 12(a)-12(b)** illustrate Bejan lines for considered values of γ and β. The variation of Bejan lines occurs closer to the hot wall for values of γ values as compared to β. Also in the neighbourhood of the hot wall, it is pinpointed that, for all values of γ and β the Bejan lines having sharpened vertex point towards the leading edge of the cylinder and move away from the wall as *R* increases. Bejan contour value shrinkages for cumulative values of γ and β. Also, Bejan lines give higher values for γ and lower values for β. With increasing values β, the Bejan lines tend to depart from the hot wall as compared to γ but there is no such variation in the case of entropy lines. Further, the Bejan number (Be) follows the same trend as that of entropy generation (*Ns*) this is due to the definition of the parameter *Be* [Refer Eq. (21)]. Also, as explained in the earlier paragraph (Figs. 8 & 9), the entropy generation (*Ns*) and its contours are not smooth near the cylinder wall. Therefore, in a similar way, the Bejan number (*Be*) curves are also not smooth near the wall which is observed in the Figs. 11 and 12.

**5.4 Comparison between Second-grade Viscoelastic and Newtonian Fluid Flows**

**Figure 13** explains the flow-field (*U* &*T*) variable contours for second-grade and Newtonian fluid flows. Fig. 13(a) denotes second-grade fluid and Fig. 13(b) corresponds to a Newtonian fluid. Here the flow of second-grade fluid velocity is perceived to be less compared to the Newtonian fluid. However, a greater temperature is attained by the second-grade fluid than the Newtonian fluid. In addition, the time-independent temperature contours for the second-grade fluid are rather dissimilar and a thicker thermal boundary layer is attained related with the Newtonian fluid.

**6. Concluding remarks**

The entropy generation in time-dependent buoyancy-driven thermal convection boundary layer flow of a second-grade fluid from a vertical cylinder with viscosity variation and viscous dissipation has been analysed numerically. A stable Crank-Nicolson implicit finite difference scheme is used to elucidate governing conservation equations under well-posed initial and boundary conditions. The results obtained from this research may be summarized as follows:

- The required time to complete the steady-state decreases as viscoelastic parameter ($\beta$) or temperature-dependent viscosity ($\gamma$) are enhanced, and the opposed behaviour is induced with augmenting viscous dissipation parameter ($\varepsilon$).
- Both velocity and temperature increases with escalating values of viscoelastic parameter ($\beta$) or temperature-dependent viscosity ($\gamma$) and the opposite response is noticed with an increase in dissipation parameter ($\varepsilon$).
- Skin friction ($\overline{C_f}$) and wall heat transfer rate ($\overline{Nu}$) are reduced with increasing values of all values of the control parameters.
- Entropy heat generation number decreases for increasing values of temperature-dependent viscosity and viscoelastic parameter. The opposite trend is induced with increasing Grashof number, group parameter and Prandlt number.
- Bejan number increases for all the cumulative values of control parameter except Prandtl number, $Pr$.

The current study has revealed important thermodynamic and heat transfer features associated with external thermal convection boundary layer flows of viscoelastic dilute polymer suspensions. Future studies will explore other non-Newtonian models e.g. the Oldroyd-B viscoelastic model and will be communicated imminently.

**References**

1. Gebhart, B., Jaluria, Y., Mahajan, R. L., and Sammakia, B. *Buoyancy-Induced Flows and Transport*, Hemisphere, New York (1988).

2. Chhabra, R. P. Fluid Flow and Heat Transfer from Circular and Noncircular Cylinders Submerged in Non-Newtonian Liquids. *Advances in Heat Transfer* Volume 43, 289-417 (2011).

3. Mitsoulis, E. and Galazoulas, S., Simulation of viscoplastic flow past cylinders in tubes. *Journal of Non-Newtonian Fluid Mechanics* 158, 132–141(2009).

4. Chhabra, R. P., Soares, A. A. and Ferreira, J. M., Steady non-Newtonian flow past a circular cylinder: A numerical study. *Acta Mechanica* 172, 1–16 (2004).

5. Prasad, V.R. Abdul Gaffar, S., Keshava Reddy, E. and Bég, O. A., Flow and heat transfer of Jefferys non-Newtonian fluid from a horizontal circular cylinder, AIAA J. Thermophysics and Heat Transfer, 28, 764-770 (2014).

6. Subba Rao, A., Amanulla, CH., Nagendra, N., Bég, O. A., and Kadir, A. Hydromagnetic flow and heat transfer in a Williamson non-Newtonian fluid from a horizontal circular cylinder with Newtonian heating, Int. J. Appl. Comp. Mathematics. (2017)doi:10.1007/s40819-017-0304-x

7. Bég, O. A., Subba Rao, A., Nagendra, N., Amanulla, CH., Reddy, M.S.N and Kadir, A. Numerical study of hydromagnetic non-Newtonian nanofluid transport phenomena from a horizontal cylinder with thermal slip: aerospace nanomaterial enrobing simulation, *J. Nanofluids,* 7, 1–14 (2018).

8. Kairi, R. R., Murthy, P. V. S. N. and Ng, C. O. Effect of viscous dissipation on natural convection in a non-Darcy porous medium saturated with non-Newtonian fluid of variable viscosity. *The Open Transport Phenomena Journal* 3, 1–8(2011).

9. Ragueb, H. and Mansouri, K., A numerical study of viscous dissipation effect on non-Newtonian fluid flow inside elliptical duct. *Energy Conversion and Management* 68, 124–132 (2013).

10. Manglik, R. M. and Prusa, J., Viscous dissipation in non-Newtonian flows: Implications for the Nusselt number. *AIAA Journal of Thermophysics and Heat Transfer* 9, 733–742(1995).

11. Shamshuddin, M. D., Bég, O. A., Surinder Ram, M., and Kadir, A., Finite element computation of multi-physical micropolar transport phenomena from an inclined moving plate in porous media, *Indian J. Physics* (2017). doi.org/10.1007/s12648-017-1095-y

12. Ali, N., Zaman, A., Bég, O. A., Hayat, T., Mathematical model for isothermal wire-coating from a bath of Giesekus viscoelastic fluid, *Chem. Eng. Comm.* 203, 1336-1248(2016).

13. Zaib, A., K. Bhattacharyya, M. Sharif Uddin, and S. Shafie (2016). Dual solutions of non-Newtonian Casson fluid flow and heat transfer over an exponentially permeable shrinking sheet with viscous dissipation. *Modelling and Simulation in Engineering*, 2016, 1–8.

14. Barletta, A. Fully developed laminar forced convection in circular ducts for power law fluids with viscous dissipation. *Int. Journal of Heat and Mass Transfer* 40, 15–26 (1997).

15. Coleman, B. D. and Noll, W. An approximation theorem for functionals, with applications in continuum mechanics, *Arch. Rat. Mech. Anal.* 6, 355-370 (1960).

16. McTigue, D. F., S. L. Passman, and S. J. Jones. Normal stress effects in the creep of ice. *Journal of Glaciology* 38, 120–126 (1985).

17. Das, K. Influence of chemical reaction and viscous dissipation on MHD mixed convection flow. *Journal of Mechanical Science and Technology* 28, 1881–1885(2014).

18. Nadeem, S., Rehman, A., C. Lee, C. and Lee, J. Boundary Layer Flow of Second-grade Fluid in a Cylinder with Heat Transfer, *Mathematical Problems in Engineering*, 2012, 1-13(2012).

19. Hayat, T., Anwar, M. S. , Farooq, M.  and Alsaedi, A.  MHD stagnation point flow of second-grade fluid over a stretching cylinder with heat and mass transfer. *Int. J. Nonlinear Sci. Numer. Sim.* 15(6), 365–376(2014).

20. Nayak, A. and Panda, S. Mixed convective MHD flow of second-grade fluid with viscous dissipation and Joule heating past a vertical infinite plate with mass transfer, *Mathematical Theory and Modeling*, 3, 38-46(2013).

21. Sahoo, B. Effects of slip, viscous dissipation and Joule heating on the MHD flow and heat transfer of a second-grade fluid past a radially stretching sheet. *Appl. Math. Mech. -Engl. Ed.* 31(2), 159–173 (2010).

22. Majeed, A., Javed, T., and Ghaffari, A. Numerical investigation on flow of second-grade fluid due to stretching cylinder with Soret and Dufour effects. *Journal of Molecular Liquids* 221, 878–884(2016).

23. Bejan, A. Entropy Generation Optimization, CRC Press, Florida, 1996.

24. Giangaspero, G. and Sciubba, E. Application of the entropy generation minimization method to a solar heat exchanger: A pseudo-optimization design process based on the analysis of the local entropy generation maps. *Energy* 58, 52–65(2013).

25. Badescu, V. Optimal paths for minimizing lost available work during usual heat transfer processes. *J. Non-Equilib. Thermodyn.* 29, 53–73(2004).

26. Kockum, H. and A. Jernqvist, A. Entropy generation in multi-field flows: Equations and examples of applications. *Trans. IChemE* 76, 212–222(1998).

27. Rashidi, M. M., Bég, O. A and Freidooni Mehr, N. Second law analysis of hydromagnetic flow from a stretching rotating disk: DTM-Padé simulation of novel nuclear MHD propulsion systems, *Frontiers of Aerospace Engineering*, 2, 1, 29-38(2013).

28. Srinivas, J, Gajjela, N and Bég, O. A. Mathematical modelling of entropy generation in magnetized micropolar flow between co-rotating cylinders with internal heat generation, *Alexandria Engineering J.*,55, 1969-1982(2016).

29. Adesanya, S. O., Kareem, S. O., Falade, J. A. and Arekete, S. A. Entropy generation analysis for a reactive couple stress fluid flow through a channel saturated with porous material, *Energy* 93, 1239-1245(2015).

30. Akbar NS, Shoaib, M., Tripathi, D., Bhushan, S. and Bég, O. A. Analytical approach for entropy generation and heat transfer analysis of CNT-nanofluids through ciliated porous medium, *J. Hydrodynamics B*, In press(2017).

31. Aksoy, Y. Effects of couple stresses on the heat transfer and entropy generation rate for a flow between parallel plates with constant heat flux. *International Journal of Thermal Sciences*, 107, 1–12(2016).

32. Galanis, N. and Rashidi, M. M. Entropy generation in non-Newtonian fluids due to heat and mass transfer in the entrance region of ducts. *Heat Mass Transfer* 48, 1647–1662(2012).

33. Kahraman, A. Entropy generation due to non-Newtonian fluid flow in annular pipe with relative rotation: constant viscosity case. *Journal of Theoretical and Applied Mechanics* 46, 69–83(2008).

34. Sajjad-ur, R., R. ul Haq, Khan, Z. H. and Lee, C. Entropy generation analysis for non-Newtonian nanofluid with zero normal flux of nanoparticles at the stretching surface. *Journal of the Taiwan Institute of Chemical Engineers* 63, 226–235(2016).

35. Butt, A. S., Munawar, S., Mehmood, A. and Ali, A. Effect of viscoelasticity on entropy generation in a porous medium over a stretching plate. *World Applied Sciences Journal*, 17, 516–523(2012).

36. Yilbas, B. S. and Pakdemirli, M. Entropy generation due to the flow of a non-Newtonian fluid with variable viscosity in a circular pipe. *Heat Transfer Engineering* 26, 80–86(2005).

37. Yurusoy, M., Bayrakoekem, H., Kapucu, M. and Aksoy, F. Entropy analysis for third grade fluid flow with Vogel's models of viscosity in annular pipe. *International Journal of Non-Linear Mechanics*, 43, 588–599(2008).

38. Kahraman, A. and Yurusoy, M. Entropy generation due to non-Newtonian fluid flow in annular pipe with relative rotation: constant viscosity case. *Journal of Theoretical and Applied Mechanics* 46, 69–83(2008).

39. Chauhan, D. S. and Kumar, V. Entropy analysis for third-grade fluid flow with temperature-dependent viscosity in annulus partially filled with porous medium. *Theoret. Appl. Mech* 40, 441–447(2013).

40. Xu, B. et al. Viscous dissipation influencing viscosity of polymer melt in micro channels, *Journal of Mechanical Science and Technology*, 24, 1417–1423(2010).

41. Fosdick, R. L. and Rajagopal, K. R. Uniqueness and drag for fluids of second-grade in steady motion. *International Journal of Non-Linear Mechanics* 13, 131–137(1978).

42. Rajagopal, K. R. and Gupta, A. S. An exact solution for the flow of a non-Newtonian fluid past an infinite porous plate. *Meccanica* 19, 156–160(1974).

43. Dunn, J. E. and Rajagopal, K. R. Fluids of differential type: critical review and thermodynamic analysis. *International Journal of Engineering Science* 33, 689–729(1995).

44. Cengel, Y. *Fluid Mechanics Fundamentals and Applications*. New York: McGrawHill (2006).

45. Touloukian, Y. S., Saxena, S. C. and Hestermans, P. *Thermophysical properties of matter, Viscosity*. New York: The TPRC Data Series, Plenum (1975).

46. Rani, H. P., G. J. Reddy, and C. N. Kim (2013). Transient analysis of diffusive chemical reactive species for couple stress fluid flow over vertical cylinder. *Applied Mathematics and Mechanics*, 34, 985–1000.

47. Mohiddin, S. G., Prasad, V. R. and Bég, O. A. Numerical study of unsteady free convective heat and mass transfer in a Walters-B viscoelastic flow along a vertical cone, *Int. J. Applied Mathematics and Mechanics*, 6, 88-114(2010)..

48. Prasad, V.R., Vasu, B., Bég, O. A. and Parshad, R. Unsteady free convection heat and mass transfer in a Walters-B viscoelastic flow past a semi-infinite vertical plate: a numerical study, *Thermal Science-International Scientific Journal*, 15, 2, S291-S305(2011).

49. Rajesh, V., and Bég, O. A. MHD transient nanofluid flow and heat transfer from a moving vertical cylinder with temperature oscillation, *Computational Thermal Sciences*, 6, 439-450(2014).

50. Rajesh, V., and Bég, O. A. and Mallesh, M. P. Transient nanofluid flow and heat transfer from a moving vertical cylinder in the presence of thermal radiation: Numerical study, *Proc. IMECHE- Part N: J. Nanoengineering and Nanosystems*, 230 (1) 3–16(2016).

51. Lee, H. R., Chen, T. S. and Armaly, B. F. Natural convection along slender vertical cylinder with variable surface temperature. *ASME Journal of Heat Transfer* 110, 103–108(1988).

52. Mustafa, N, Asghar, S and Hossain, M.A., Natural Convection Flow of Second-Grade Fluid Along a Vertical Heated Surface with Power-Law Temperature, Chem. Eng. Comm., **195**, 209-228, (2008).

53. Gebhart, B. Effects of viscous dissipation in natural convection, *J. Fluid Mechanics*, 14, 225–232(1962).

54. Bég, O. A., Takhar, H. S., Bharagava, R., Rawat, S. and Prasad, V.R. Numerical study of heat transfer of a third grade viscoelastic fluid in non-Darcian porous media with thermophysical effects, *Physica Scripta,* 77, 1-11(2008).

55. Bejan, A. The concept of irreversibility in heat exchanger design: Counter flow heat exchangers for gas-to-gas applications. Transactions of the ASME - J. Heat Transfer, 99, 374–380 (1977).

56. Paoletti, S., Rispoli, F. and Sciubba, E. Calculation of exergetic losses in compact heat exchanger passages, ASME AES, Vol. 10 pp. 21-29(1989).

57. Ozkol, I., Komurgoz, G. and Arıkoglu, A. "Entropy generation in laminar natural convection from a constant temperature vertical plate in an infinite fluid", Proc. IMechE, Vol. 221 Part A: J. Power and Energy, 609-616 (2007).

58. Mahmud, S. and Fraser, R. A. The second law analysis in fundamental convective heat transfer problems. Int. J. Thermal Sci., 42, 177–186 (2003).

59. Mohammad R. M. and Javad A. E. "Entropy generation analysis of free convection from a constant temperature vertical plate using similarity solution", Thermal Science, 20, 1855-1866 (2016).

| Grid size | Average Nusselt number ($\overline{Nu}$) for Pr = 0.71, $\gamma = 1.0$, β = 1.0, ε = 1.0 |
|---|---|
| 25 x 125 | 0.708685 |
| 50 x 250 | 0.688729 |
| 100 x 500 | 0.677087 |
| 200 x 1000 | 0.677041 |

**Table 1.** Grid independence test for selecting mesh size with fixed $\Delta t = 0.01$.

| Time step size ($\Delta t$) | Average Nusselt number ($\overline{Nu}$) for Pr = 0.71, $\gamma = 1.0, \beta = 1.0, \varepsilon = 1.0$ |
|---|---|
| 0.5 | 0.677375 |
| 0.1 | 0.677375 |
| 0.08 | 0.677374 |
| 0.05 | 0.677303 |
| 0.02 | 0.677221 |
| 0.01 | 0.677087 |

**Table 2.** Time independence test for selecting time step size with fixed 100 x 500 grid.
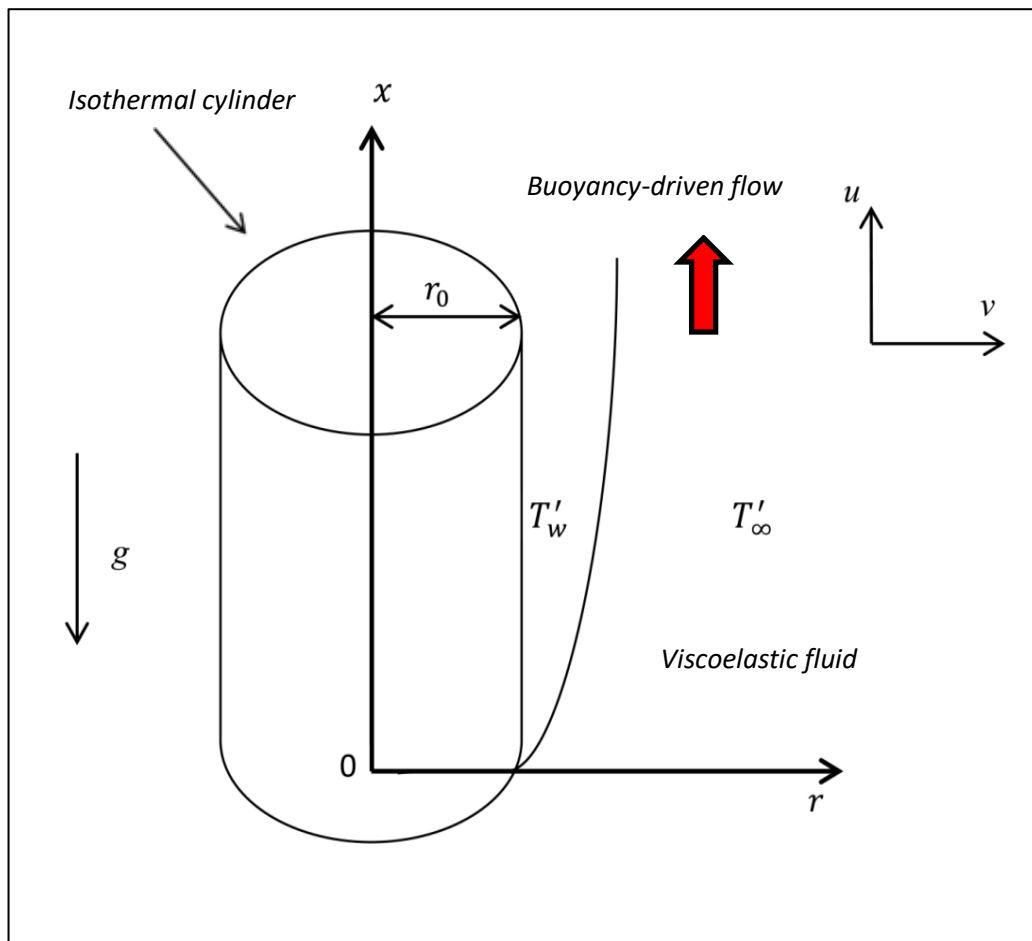
**Fig. 1**. Physical model of the analysis.
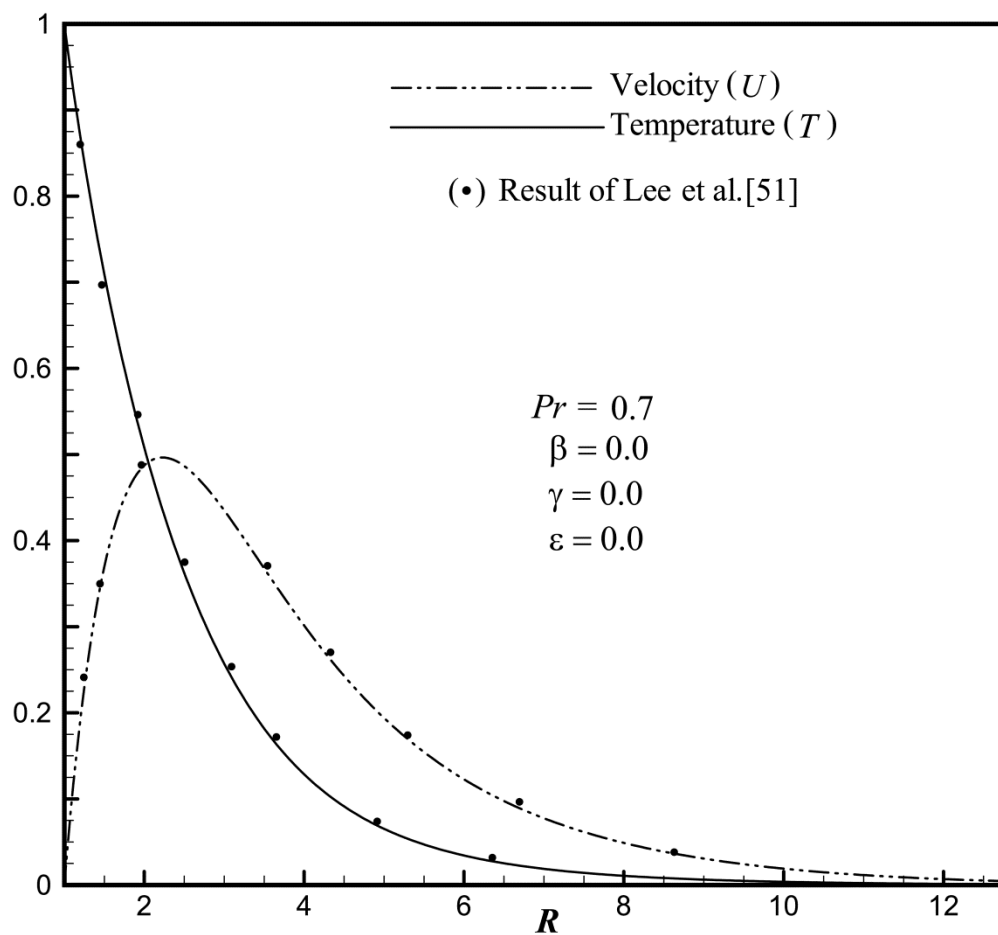
**Fig. 2.** Comparison of the flow-field variables with existing available results Lee et al. [51].
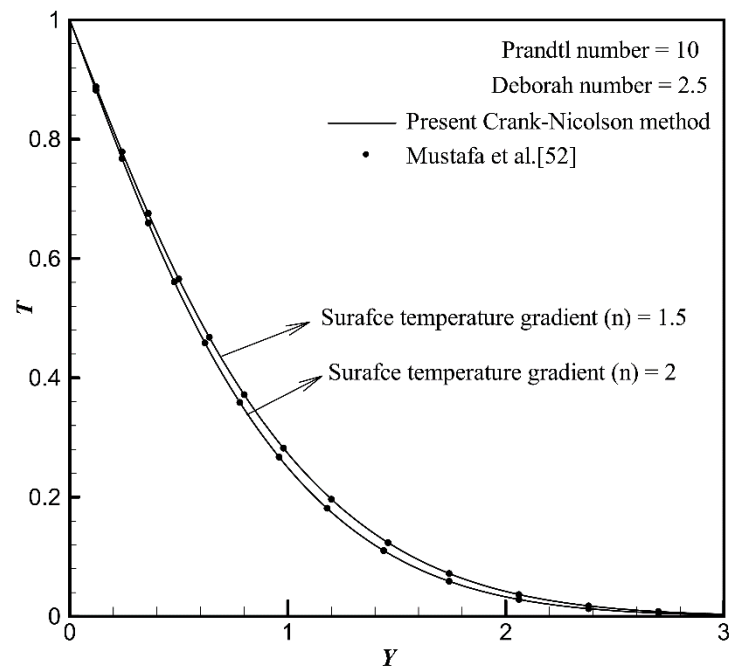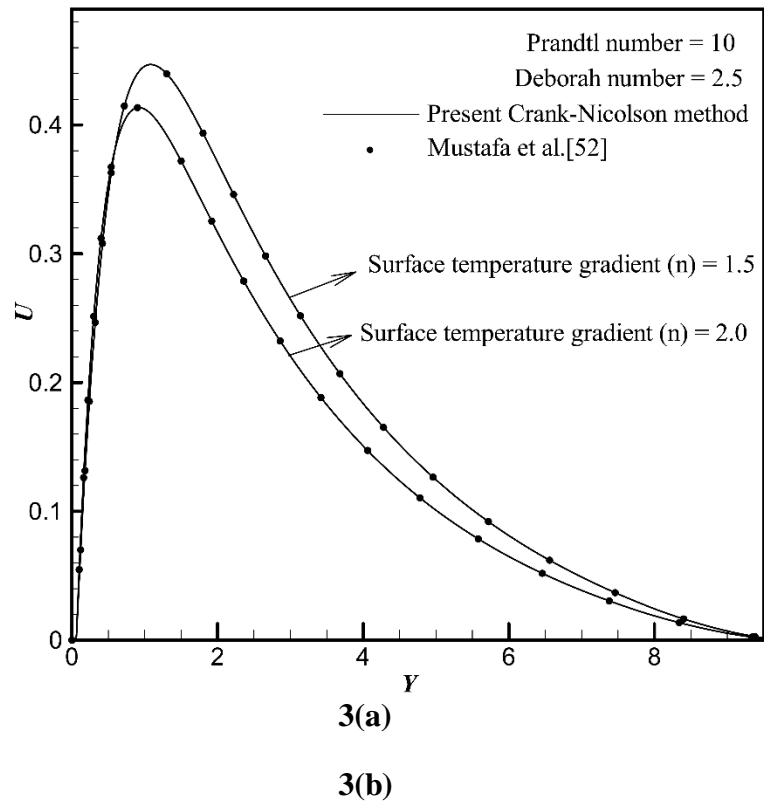
**Fig 3.** Validation of Crank-Nicolson code for second-grade fluid model (Mustafa et al. [52]) with respect to (a) velocity profile; (b) temperature profile.
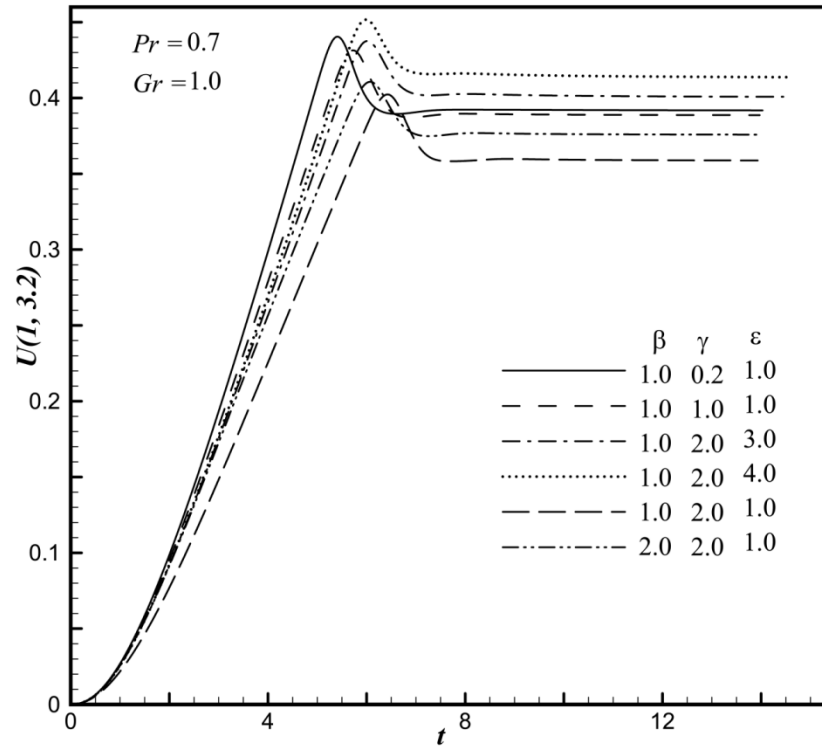
**4(a)**
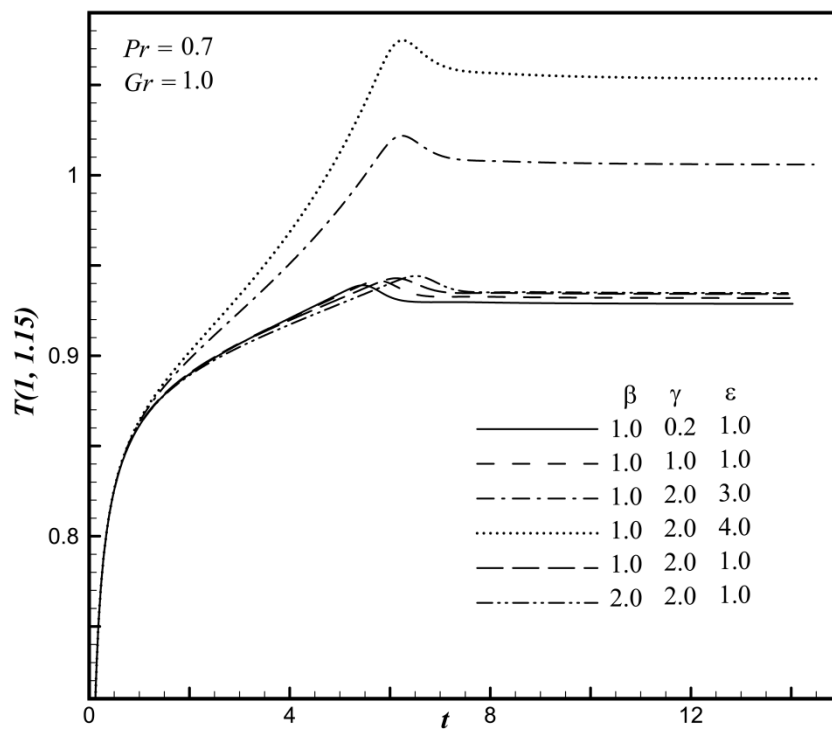


**4(b)**

**Fig. 4**. Time-dependent (a) velocity profile (*U*) at the location (1, 3.2); and (b) temperature profile (*T*) at the location (1,1.15) versus time (*t*) for various values of β, γ and ε.
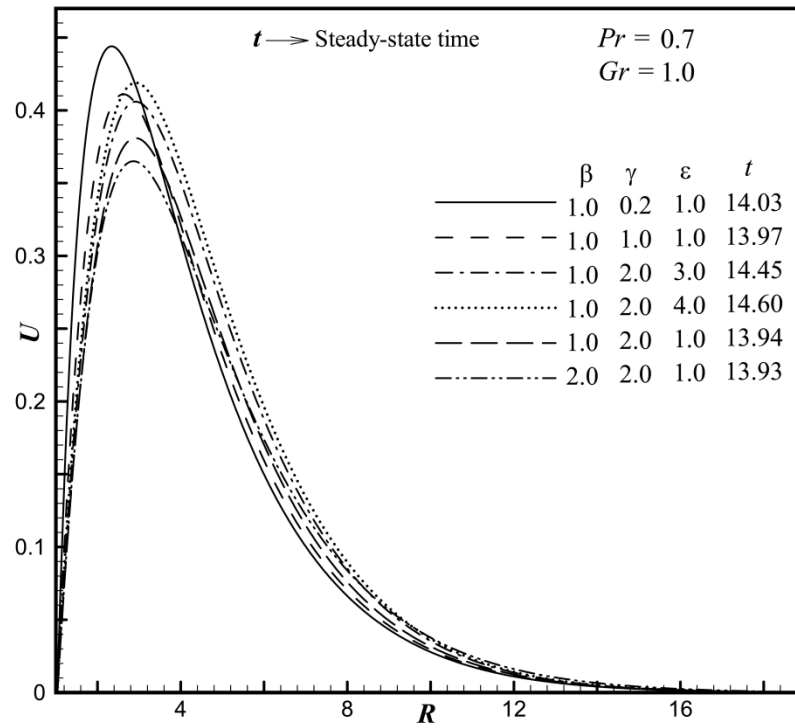
**5(a)**
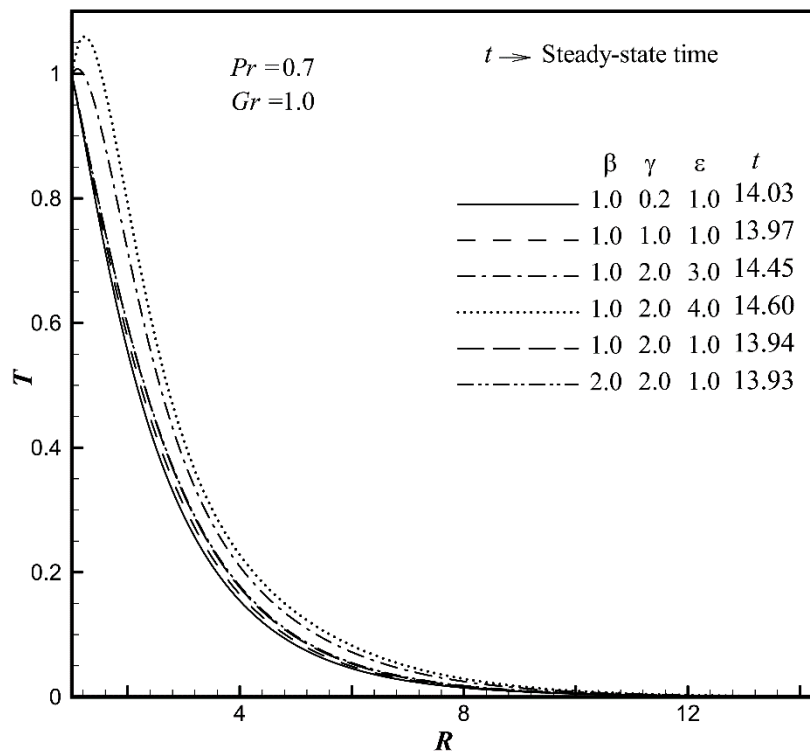


**5(b)**

**Fig. 5**. Simulated time-independent state (a) velocity ($U$); and (b) temperature ($T$) profiles versus $R$ at $X = 1.0$ for various values of $\beta$, $\gamma$ and $\varepsilon$.
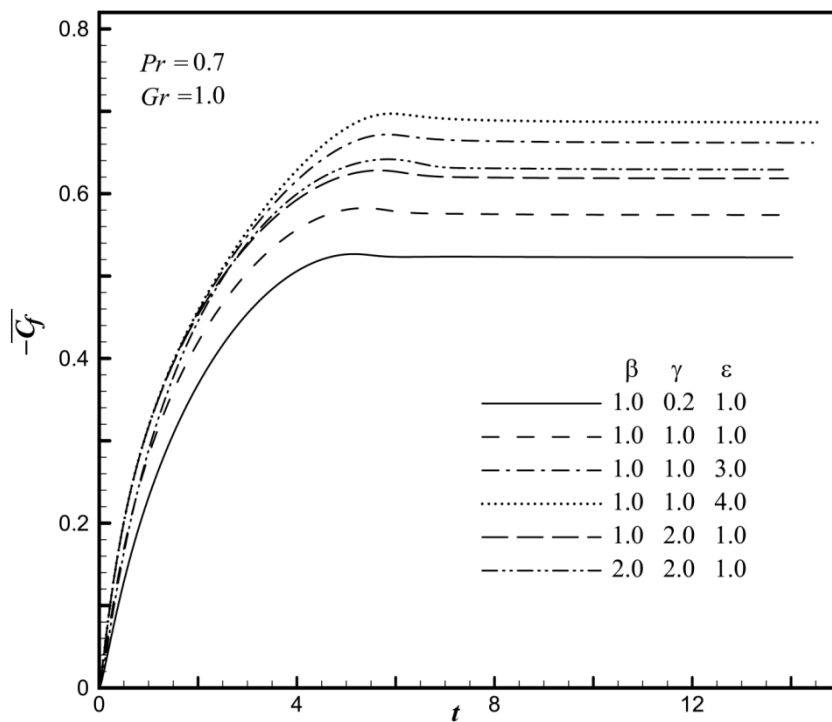
**6(a)**
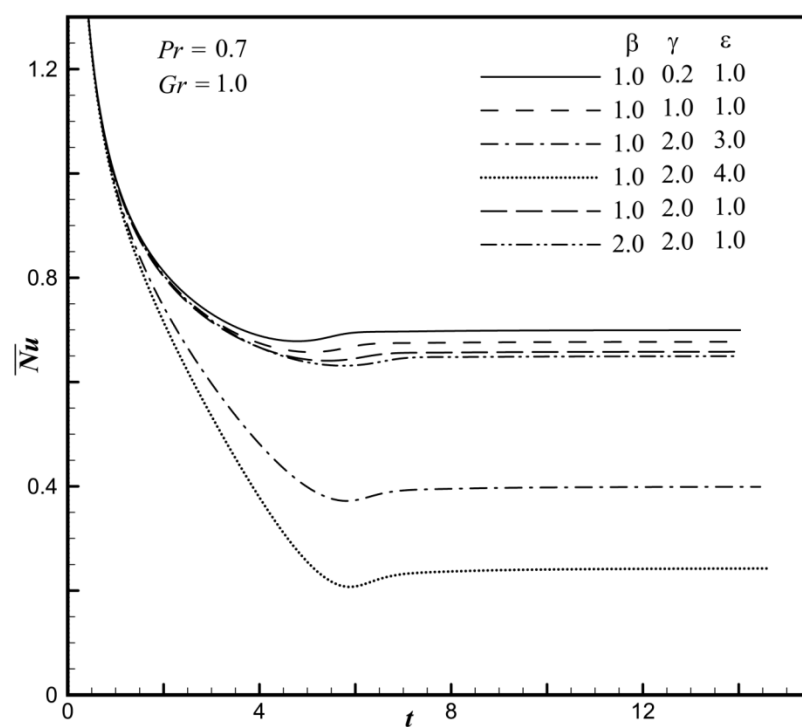


**6(b)**

**Fig. 6.** Average (a) skin-friction ($\overline{C_f}$); and (b) heat transport ($\overline{Nu}$) coefficients for distinct values of β, γ and ε.
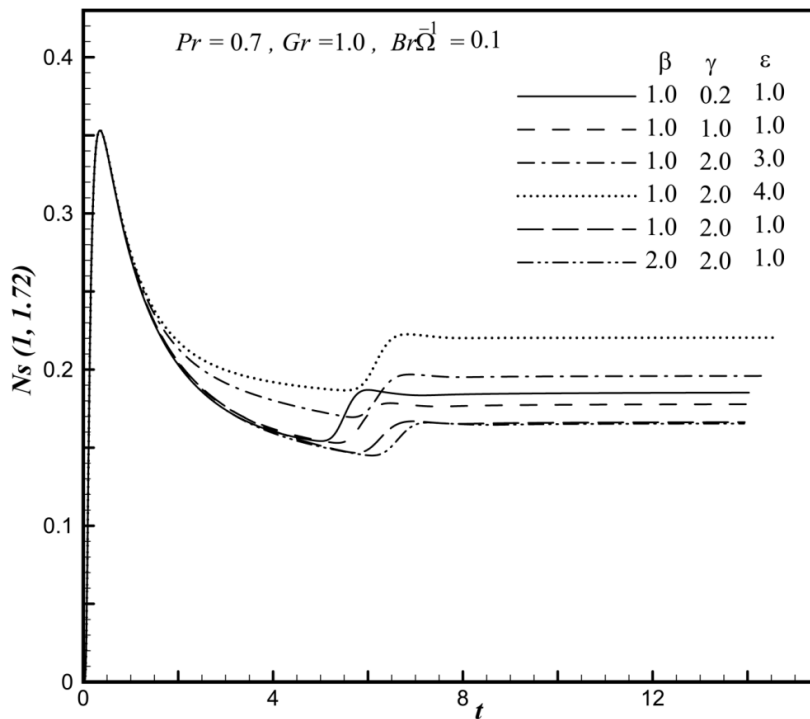
**7(a)**
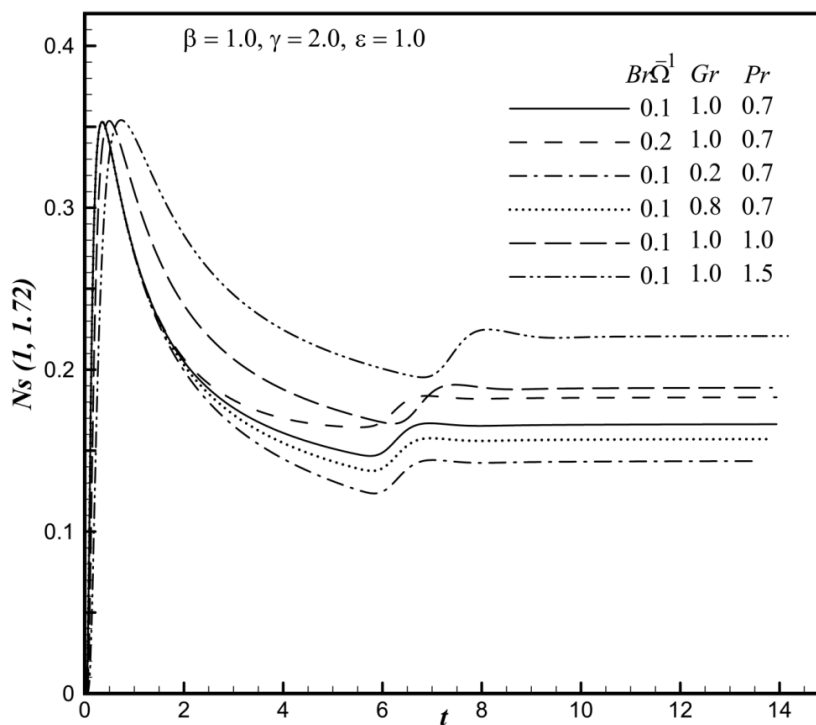


**7(b)**

**Fig. 7.** The transient entropy generation number (*Ns*) against time (*t*) for different values of (a) β, γ and ε; & (b) $Br\Omega^{-1}$, *Gr* and *Pr*.
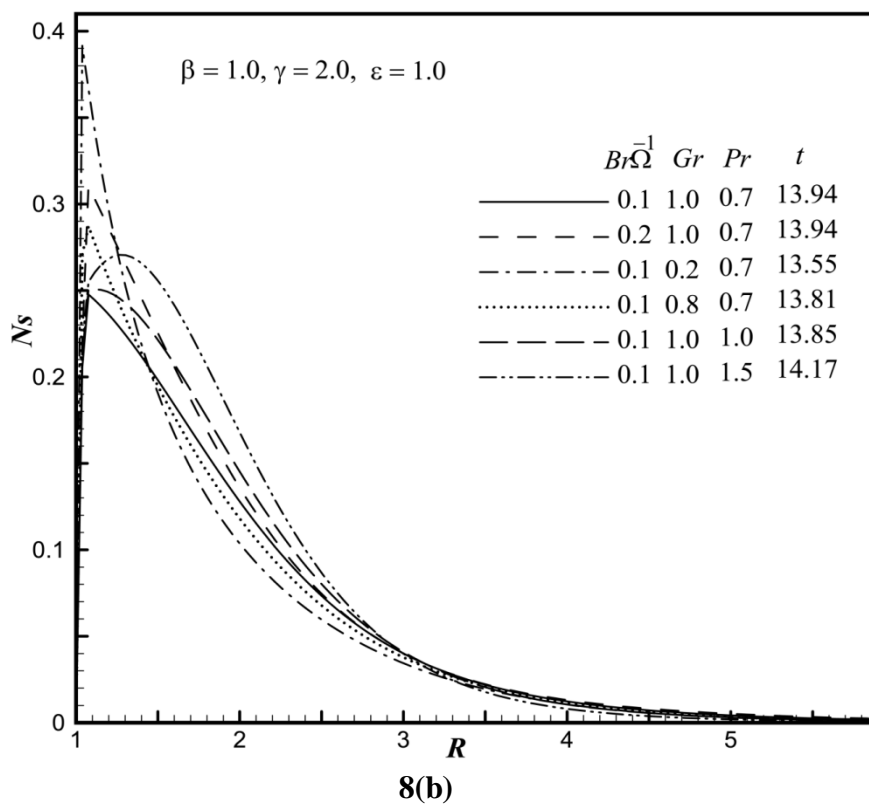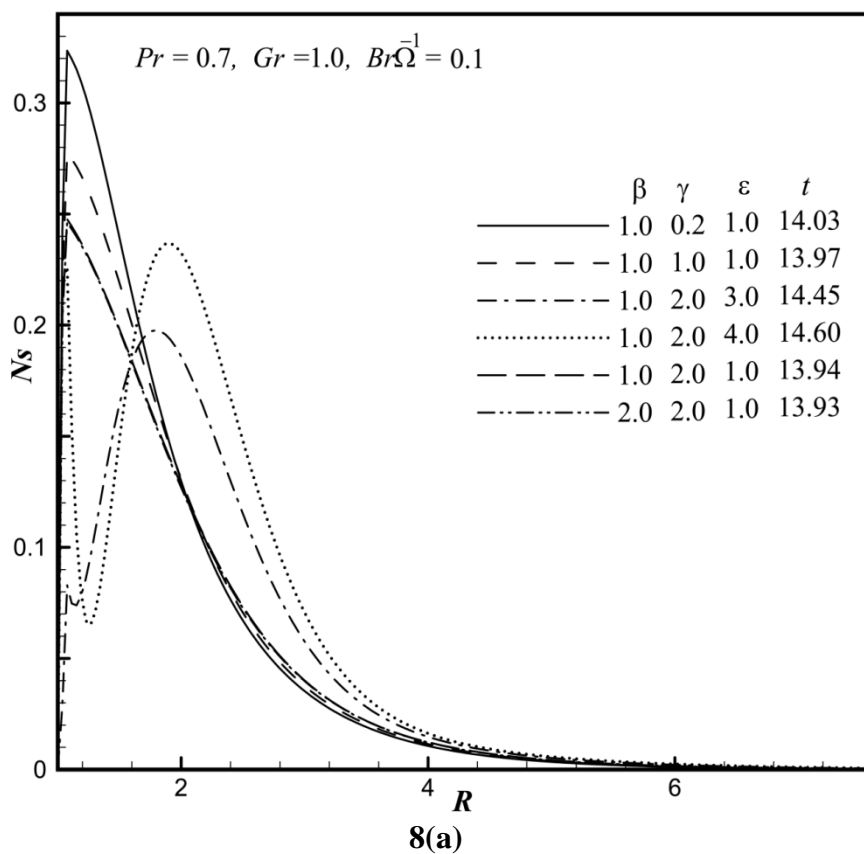
**Fig. 8.** The steady-state entropy generation number (*Ns*) against *R* at *X* = 1.0 for different values of (a) β, γ and ε; & (b) $Br\Omega^{-1}$, *Gr* and *Pr*.
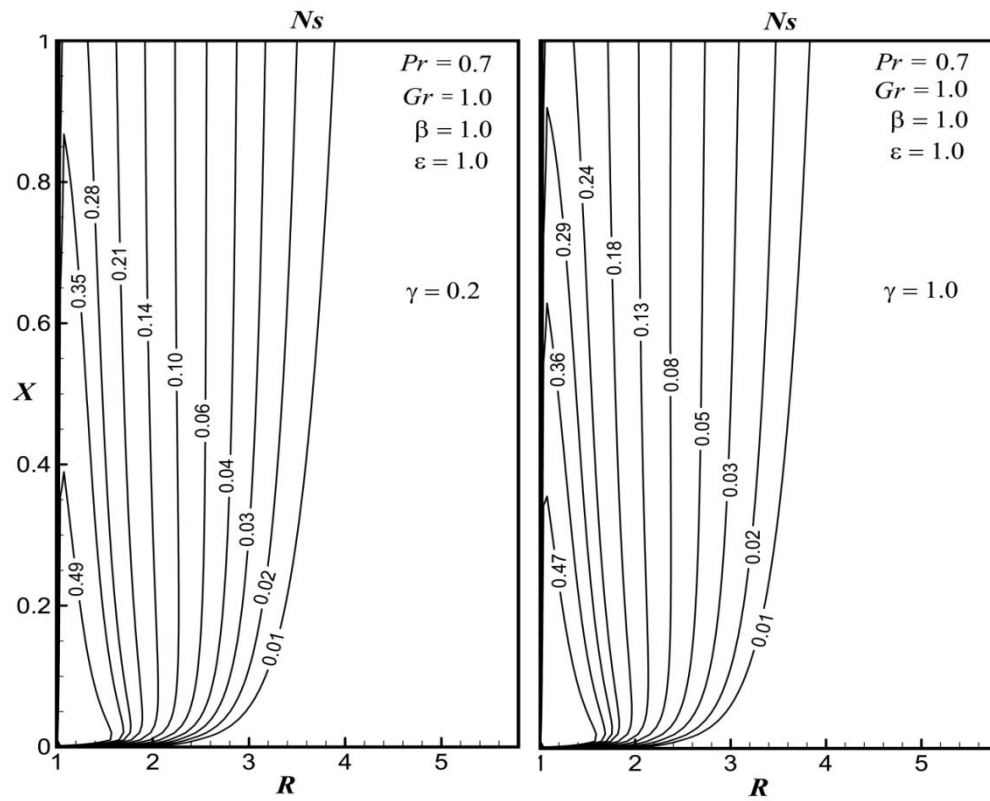
**9(a)**
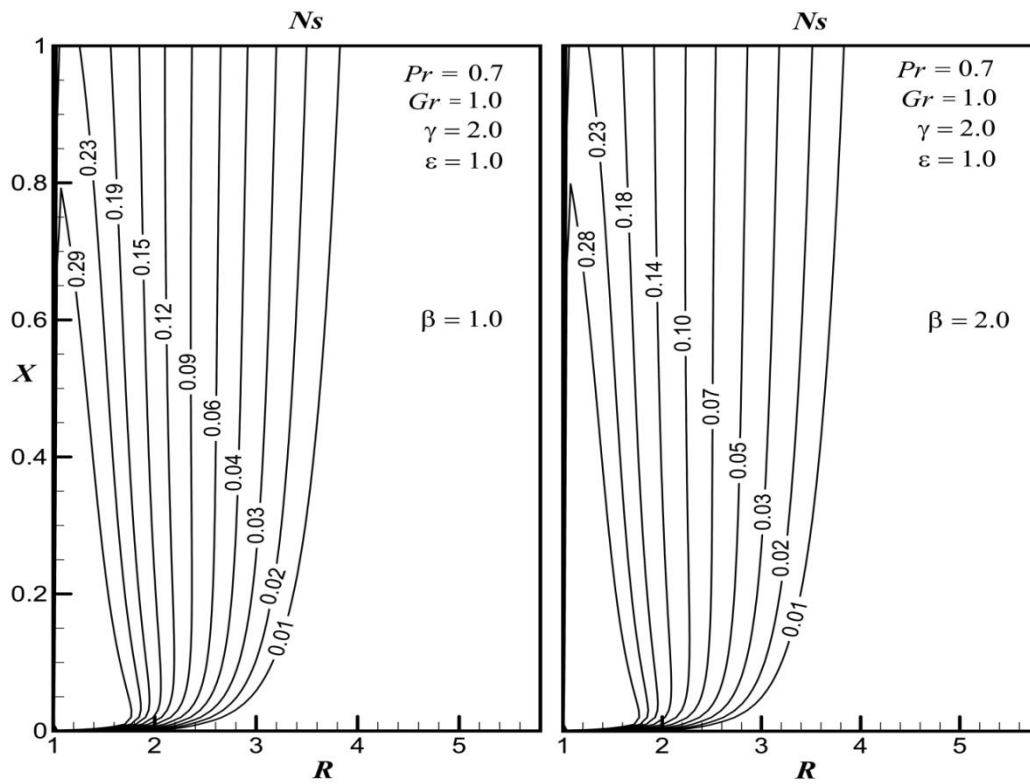


**9(b)**

**Fig. 9**. The steady-state entropy contours (*Ns*) for different values of (a) γ; and (b) β.

10(a)



10(b)
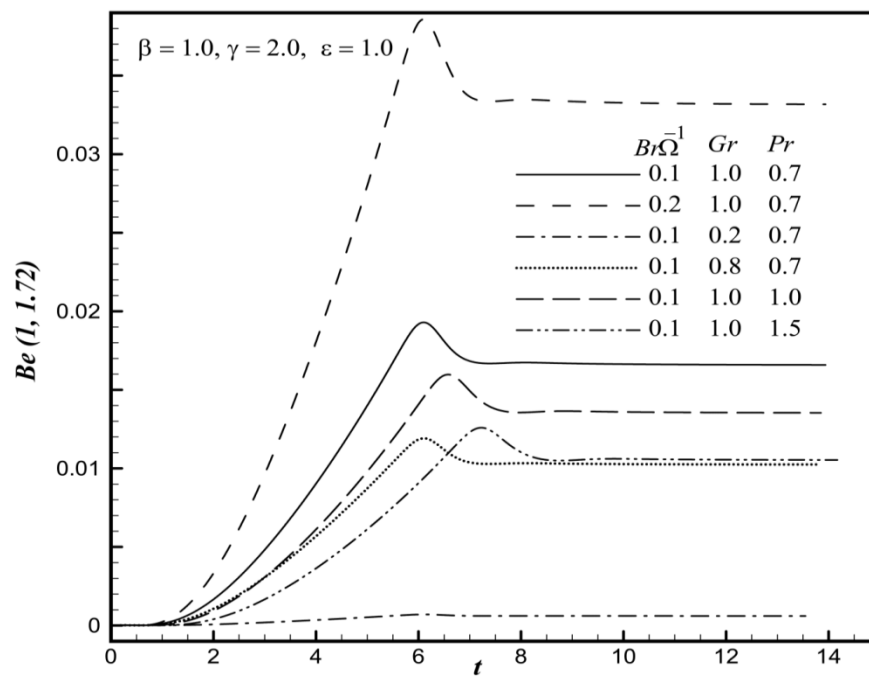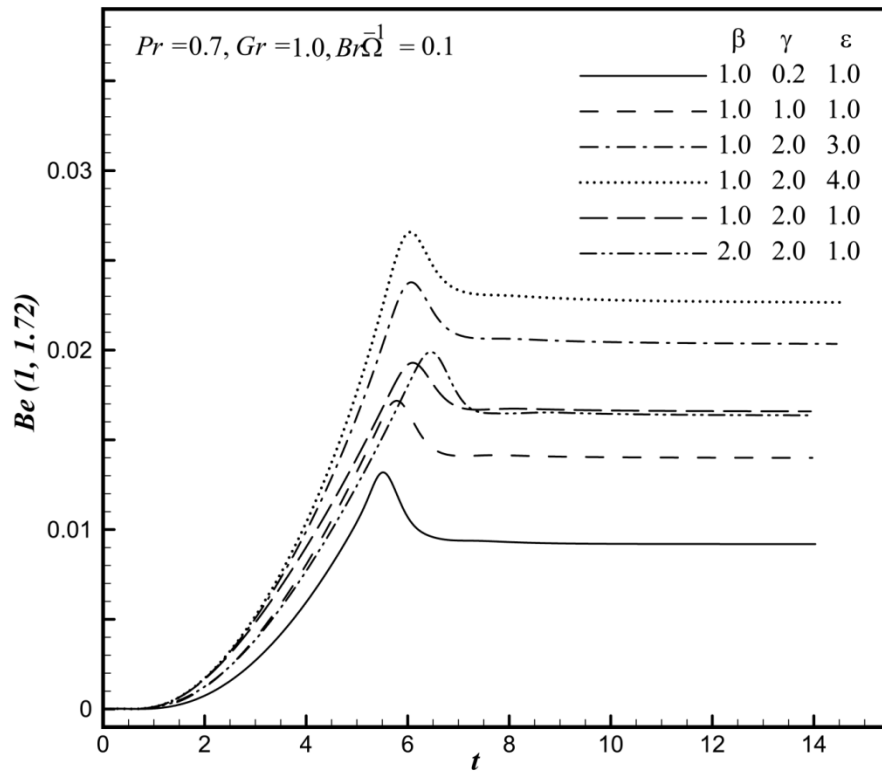
**Fig. 10.** The transient Bejan number (*Be*) against time (*t*) for different values of (a) β, γ and ε; & (b) $Br\Omega^{-1}$, *Gr* and *Pr*.
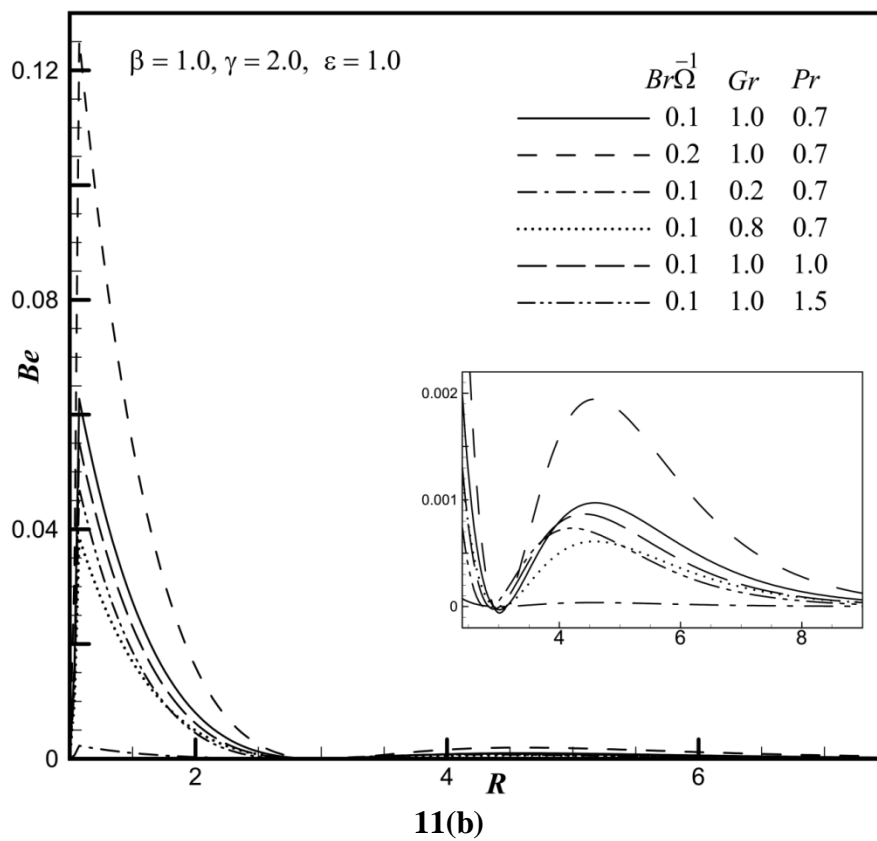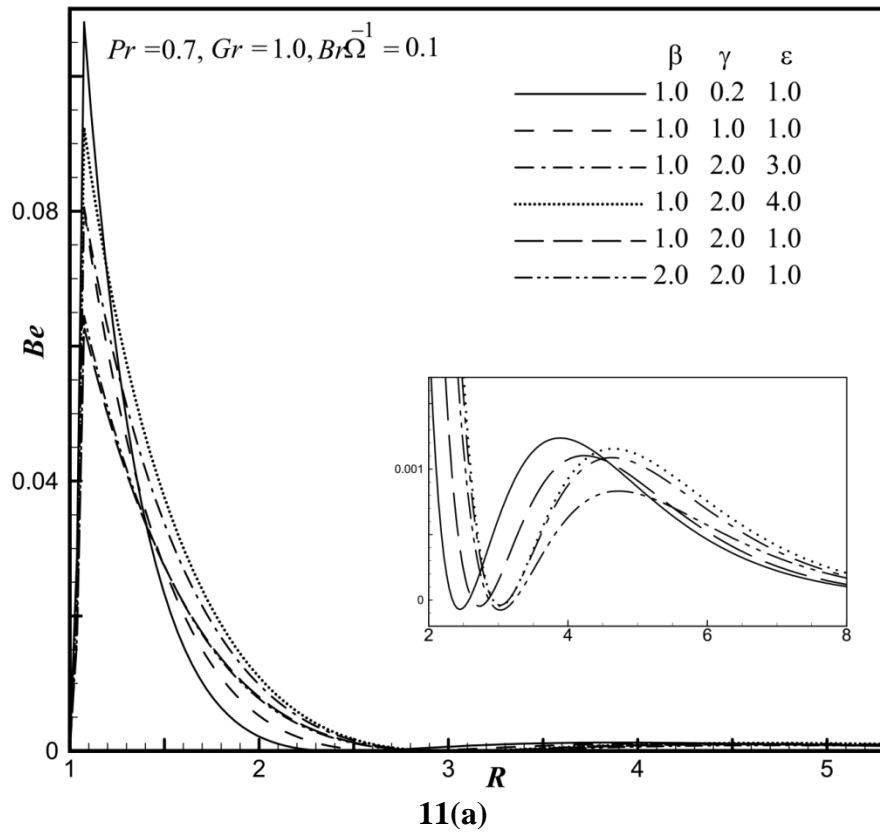
**Fig. 11.** The steady-state entropy Bejan number (*Be*) versus *R* at *X* = 1.0 for various values of (a) β, γ and ε; & (b) $Br\Omega^{-1}$, *Gr* and *Pr*.

**Be**

**Be**

$Pr = 0.7$
$Gr = 1.0$
$\beta = 1.0$
$\varepsilon = 1.0$

$\gamma = 0.2$

$Pr = 0.7$
$Gr = 1.0$
$\beta = 1.0$
$\varepsilon = 1.0$

$\gamma = 1.0$

**12(a)**

**Be**

**Be**

$Pr = 0.7$
$Gr = 1.0$
$\gamma = 2.0$
$\varepsilon = 1.0$

$\beta = 1.0$

$Pr = 0.7$
$Gr = 1.0$
$\gamma = 2.0$
$\varepsilon = 1.0$

$\beta = 2.0$
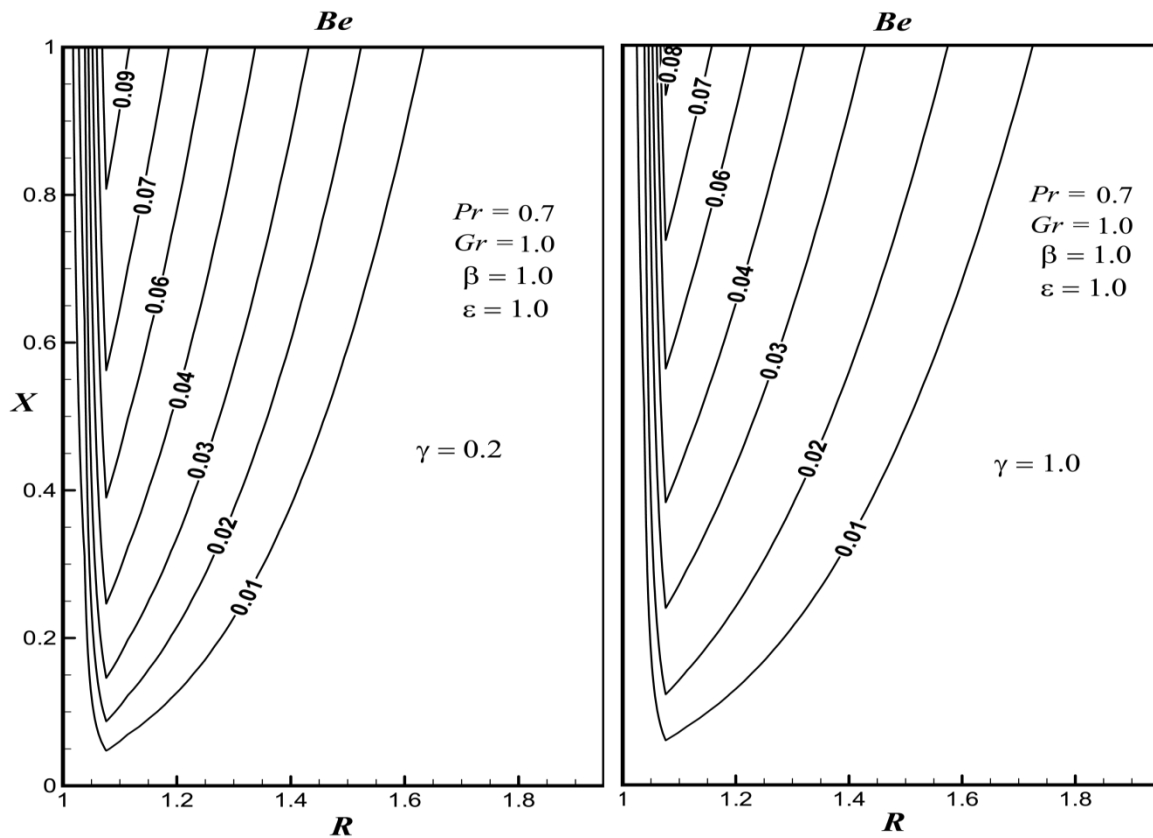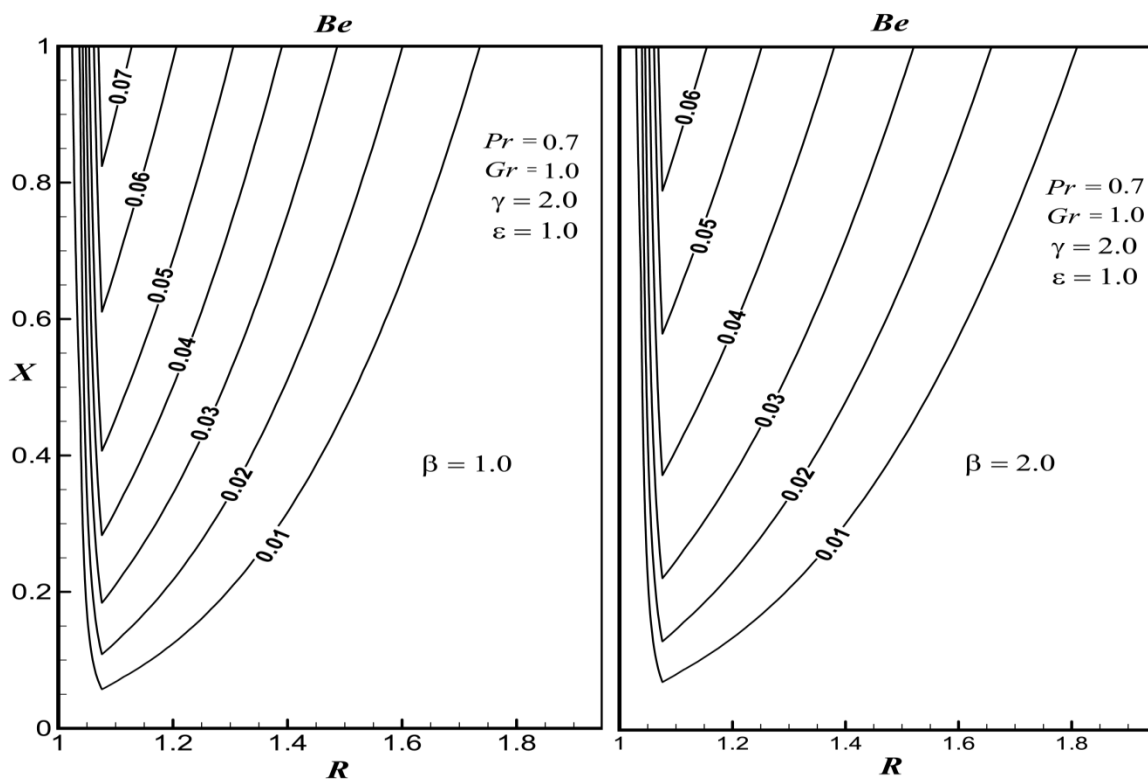
**12(b)**

**Fig. 12.** The steady-state Bejan contours (*Be*) for different values of (a) γ; and (b) β.
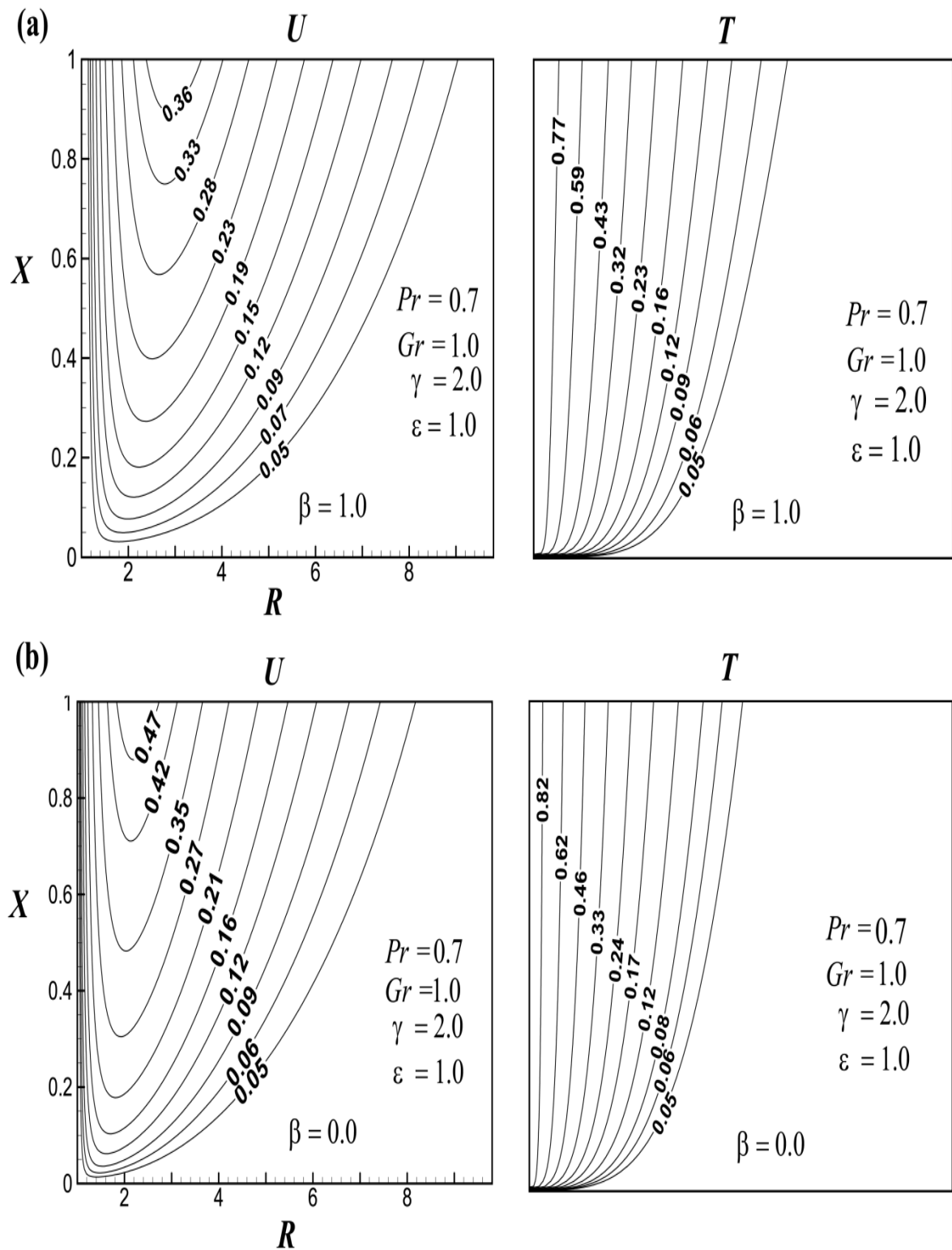
**Fig. 13.** The steady-state velocity ($U$) and temperature ($T$) contours for different values of (a) second-grade fluid ($\beta = 1.0$); and (b) Newtonian fluid ($\beta = 0.0$).